Brown carbon emissions from laboratory combustion of Eurasian

arctic-boreal and South African savanna biomass

3

1

2

- Arya Mukherjee¹, Anni Hartikainen¹, Markus Somero¹, Viljami Luostari¹, Mika Ihalainen¹, 4
- Christopher P. Rüger², Timo Kekäläinen³, Ville H. Nissinen³, Luis M.F. Barreira⁴, Hanna Koponen¹, 5
- Tuukka Kokkola¹, Delun Li^{4,9}, Lejish Vettikkat⁵, Pasi Yli-Pirilä¹, Muhammad Shahzaib¹, Meri M. 6
- Ruppel⁴, Ville Vakkari^{4,6}, Kerneels Jaars⁶, Stefan J. Siebert⁷, Angela Buchholz⁵, Kajar Köster⁸, Pieter 7
- G. van Zyl⁶, Hilkka Timonen⁴, Niko Kinnunen³, Janne Jänis³, Annele Virtanen⁵, Aki Virkkula^{4,9}, Olli 8
- Sippula^{1,3} 9

10

- 11 ¹ Department of Environmental and Biological Sciences, University of Eastern Finland, Kuopio, Finland
- 12 ²Joint Mass Spectrometry Centre, Department of Analytical and Technical Chemistry, University Rostock, Rostock,
- 13 Germany
- 14 ³Department of Chemistry and Sustainable Technology, University of Eastern Finland, Joensuu, Finland.
- 15 ⁴Atmospheric composition research unit, Finnish Meteorological Institute, Helsinki, 00101, Finland
- 16 ⁵Department of Technical Physics, University of Eastern Finland, Kuopio, Finland.
- 17 ⁶Atmospheric Chemistry Research Group, Chemical Resource Beneficiation, North-West University, Potchefstroom,
- 18 South Africa.
- 19 ⁷Unit for Environmental Sciences and Management, North-West University, Potchefstroom, South Africa.
- 20 ⁸Department of Environmental and Biological Sciences, University of Eastern Finland, Joensuu, Finland
- 21 ⁹Institute for Atmospheric and Earth System Research, University of Helsinki, Helsinki, 00014, Finland 22
- - 23 Correspondence to: Arya Mukherjee (arya.mukherjee@uef.fi) and Olli Sippula (olli.sippula@uef.fi)

24 25

Abstract:

- Warming climate is predicted to increase forest fires which can be a major source of black and brown carbon 26
- 27 (BC and BrC) into the atmosphere. Unlike North American forest fires, very limited studies have
- characterized North Eurasian biomass burning (BB) emissions. In this work, we determined the emission 28
- factors (EF) of carbonaceous aerosols and characterized light absorption of BrC emitted from boreal and peat 29
- burning through offline filter extraction method. The results were compared to African savanna emissions. 30
- Effects of atmospheric dilution and oxidative aging on BrC absorptivity were investigated for selected BB 31
- 32 emissions sampled into an environmental chamber. Organic carbon (OC) and elemental carbon (EC) EFs of
- fresh BB emissions ranged between 1.30-89.9 g kg⁻¹ and 0.01-4.80 g kg⁻¹ respectively. Methanol soluble OC 33
- (MSOC) represented more than 92% of fresh BB emissions, irrespective of fuel type, and consisted of 34
- weakly absorbing BrC with imaginary refractive index at 550 nm (k_{MSOC} 550) ranging from 0.002 to 0.011. 35
- Water soluble OC (WSOC) fractions varied among fresh BB emissions but overall exhibited higher mass 36
- absorption efficiencies at 365 nm (MAE₃₆₅) than MSOC. Dilution-related evaporative loss in environmental 37

chamber resulted in less volatile OC, making them less soluble in methanol. Photochemical and dark oxidative aging further increased the low volatility OC fractions of the organics along with its oxidation state. Our estimated OC-EC emission factors and k_{MSOC} for fresh BB emissions can be used for future modelling purposes. Further online measurements are needed to account for non-soluble strong BrC in aged BB emissions.

43 44

45

46

47

48

49

50

51

52

53

54

55

56

57

58

59

60

61

62

63

64

38

39

40

41

42

Introduction:

Biomass burning (BB) emission is one of the largest anthropogenic sources of black (BC) and brown carbon (BrC) in the atmosphere (Bond et al., 2004; Kirchstetter et al., 2004). Multiple studies have predicted that open BB emissions such as wildfires will become more prevalent in the future with the warming climate, with increasing boreal forest and peatland fires threatening also the Eurasian regions (Krawchuk et al., 2009; Costa et al., 2020; Feyen et al., 2020). Along with the expected overall increase in the frequency of "high-toextreme" wildfires in Europe (de Rigo et al., 2017) an expected shift in vegetation distribution from Southern towards Northern Europe may further amplify fire hazard of Fenno-Scandinavian biomass (Costa et al., 2020). Only limited laboratory and field studies exist describing aerosol emissions from boreal forest and peatland fires in the Eurasian area (Wilson et al., 2015;McCarty et al., 2021;Zhong et al., 2024; Schneider et al., 2024a), compared to the more studied North-American boreal forest and peat fires (Aurell and Gullett, 2013; Urbanski, 2013; Stockwell et al., 2014; Black et al., 2016; Andreae, 2019; Phillips et al., 2022; Zhao et al., 2021). However, the fire regimes in Eurasia are known to be dominated by surface burning, that likely emits carbonaceous aerosol of different characteristics in comparison to more crown-fire dominated fires in North America (De Groot et al., 2013; Rogers et al., 2015). Another important source of global carbon emissions is savanna surface fires, which has been estimated to account for almost 50% of total carbon emissions from open BB (van der Werf et al., 2017). Further, roughly 30% of the total wildfire-induced carbon emissions originate solely from Southern African savanna fires (van Wees et al., 2022). Yet, relatively limited studies have been carried out to characterize these emissions in recent years (Vakkari et al., 2014, 2018; Desservettaz et al., 2017; Wu et al., 2021; Vernooij et al., 2022, 2023).

Chemical and optical properties of BC have been studied extensively over the last two decades and it has been established as an important climate warming agent (Jacobson, 2000, 2001; Bond et al., 2013). On the other hand, the properties of combustion emitted BrC have still not been fully characterized due to variability in combustion conditions (Martinsson et al., 2015; Wang et al., 2020; Saleh, 2020), fuel chemical composition (Saleh et al., 2014; Smith et al., 2020; Moschos et al., 2024; Navinya et al., 2024) and secondary transformation of BrC in the atmosphere (Laskin et al., 2015; Brown et al., 2018; Hems et al., 2021). BB derived BrC consists of different light-absorbing organic precursors of BC, such as polyaromatic molecules, which are not transformed to fully ordered BC during the combustion process (Saleh et al., 2018). Since BC formation is strongly temperature-dependent, low combustion temperatures may favour BrC formation, whereas high combustion temperatures increase oligomerization/polymerization of polyaromatic carbon structures to form BC (Faccinetto et al., 2011; Desgroux et al., 2013; Solum et al., 2001; Wang, 2011). Consequently, the light-absorbing primary organic aerosols (POA) emitted from BB emission are chemically diverse and distinct for different fuel types and combustion conditions. Additionally, they evolve in the atmosphere through oxidation and functionalization reactions, driven by the formation of secondary organic aerosol (SOA) and the evaporation and chemical fragmentation of organic aerosol (OA), resulting in a complex mixture of organic chromophores with variable absorptivity.

BB is a dynamic and variable process that strongly depends on fuel moisture content, fuel composition and combustion conditions. A common parameter to characterize BB is the modified combustion efficiency (MCE), which describes the share of carbon dioxide to the sum of CO and CO2 emissions. However, studies have typically found only weak correlations between BrC light absorption and MCE (Pokhrel et al., 2016; McMeeking et al., 2014). The ratio of the emitted BC (mainly composed of elemental carbon or EC structures) to the organic carbon (OC) has been suggested as a more suitable parameter for correlating the aerosol optical properties with combustion conditions (McClure et al., 2020; Stockwell et al., 2016; Saleh, 2020). For instance, flaming dominated combustion processes generally lead to relatively high EC/OC ratios and more absorptive BrC than smouldering emissions (Saleh et al., 2014; Xie et al., 2018; McClure et al., 2020; Kumar et al., 2018).

In climate models, the light absorption strength of the material is described by the imaginary part of the refractive index (k). For pure BC, k- are constrained close to unity and exhibit very little to no wavelength dependence, especially at UV and shorter visible wavelengths (Bond and Bergstrom, 2006). However, the k for BB emitted BrC seem to vary across several orders of magnitude depending on the biomass type and combustion conditions as well as the measurement techniques (Chakrabarty et al., 2010; Bluvshtein et al., 2017; Saleh et al., 2018; Saleh et al., 2020; Navinya et al., 2024). Therefore, characterizing the k for individual BrC compounds is a daunting and, in some cases, impossible task due to instrumental limitations. A more comprehensive approach has been adapted in the last decade where the k values for BB derived BrC has been shown to fall in a "brown-black carbon continuum" (Saleh et al. 2018). BB derived BrC generally exhibit progressively higher k values with increasing temperature and has been termed as "dark BrC (d-BrC)" (Hoffer et al., 2017; Adler et al., 2019; Atwi et al., 2022; Chakrabarty et al., 2023) or "strongly absorptive BrC (s-BrC)" (Mclure et al., 2020; Saleh et al., 2020) when the combustion temperatures approach the BC formation regime. In contrast, the BrC derived from BB combustions in progressively decreasing combustion efficiency and temperature has been termed as "moderately absorptive (M-BrC)", "weakly absorptive (w-BrC) and "very weakly absorptive (VW-BrC)", respectively (Saleh et al., 2020; Moschos et al., 2024), as the k values decrease with lower burning temperature.

One of the most convenient and widely used methods for the characterization of optical properties of bulk BrC is the collection of aerosol particles on filters and subsequent extraction of the organic fractions with suitable solvents followed by filtration (Chen and Bond, 2010; Liu et al., 2013; Mo et al., 2017; Shetty et al., 2019; Li et al., 2020, Yan et al., 2020). The light absorption of solvent extracted OA is measured using a UV-vis spectrophotometer which provides high precision spectral data over a wide wavelength range. In previous studies water has been one of the primary solvents for extraction of BrC from filters (Bosch et al., 2014; Kirillova et al., 2014; Mukherjee et al., 2020) because of the atmospheric relevance of the water soluble organic (WSOC) fraction (Hallar et al., 2013, Taylor et al., 2017).

Quantification of WSOC can be done with Total Organic Carbon (TOC) analysis (Li et al., 2016), and the loss estimation of the extraction process has very little uncertainty. On the other hand, the water insoluble BrC fraction is generally extracted from aerosol particles using methanol (MeOH) as a solvent (Chen and

Bond, 2010) but it has been recently discovered that some highly light-absorbing, extremely low volatility organic (ELVOC) compounds may not be efficiently extracted by this procedure (Saleh et al., 2014; Liu et al., 2013). Quantifying the dissolved organic mass in MeOH is also challenging as organic solvents interfere with TOC measurements and indirect methods are used instead (Chen and Bond 2010; Cheng et al., 2017; Huang et al., 2018; Yan et al., 2020) to estimate MeOH soluble organic carbon (MSOC) which leads to additional potential sources of uncertainties (Yan et al., 2020). Nevertheless, MeOH has exhibited very high organic extraction efficiencies (Chen and Bond, 2010; Xie et al., 2017) and the optical properties of MSOC have agreed well with OC extracted by more polar solvents like Dimethylformamide (DMF) for BB emissions and coal combustion (Xu et al., 2022). Therefore, MeOH should be used in parallel to water to extract BB emitted organic compounds with a broader range of polarities and gain more information on their light-absorbing properties. Although filter based solvent extraction has its limitations, such as lack of information on size-dependent absorption of extracted organics (Moosmüller et al., 2011; Liu et al., 2013; Washenfelder et al., 2015), this analytical method is low-cost, easily accessible, and excludes the interference of BC (or EC) and other light-absorbing species from OA absorption.

This work aims to define the emission factors of carbonaceous aerosols and characterize OA optical properties for emissions originating from different open BB sources. We used a laboratory open burning setup with the objective to create conditions representing natural Eurasian forest surface fires, in which the combustion temperatures likely remain low and burning is dominated by smouldering (Rogers et al., 2015; Walker et al., 2020). Finnish boreal peat and forest surface samples, commercially available boreal peat samples, and permafrost peat from arctic Russia and Svalbard (Norway) were burned in the laboratory setup. To assess the effects of burning conditions and biomass materials on carbonaceous emission factors and their optical properties, we replicated conditions ranging from smouldering to flaming, with clearly distinct combustion behaviour and MCEs for each fuel. Furthermore, we extended the study samples to include South-African savanna biomass and North European wood stove emissions, thereby encompassing a larger range of combustion conditions. Finally, we investigated the impact of atmospheric dilution and aging on the chemical and optical properties of the organic aerosols by conducting environmental chamber experiments either under photochemical or dark aging conditions for selected biomasses. The results were

used to derive imaginary refractive indices (*k*) for OAs, allowing for their classification within the black-brown carbon continuum. The results are essential to accurately estimate the direct radiative forcing effects of biomass burning emissions in climate models.

148

145

146

147

2. Methodology:

149150

151

152

153

154

155

156

157

158

159

160

161

162

163

164

165

166

167

168

169

170

171

2.1 Combustion setup and fuels

The combustion experiments were conducted in the ILMARI laboratory of the Kuopio campus of University of Eastern Finland (https://sites.uef.fi/ilmari) using an in-house designed open combustion appliance. The appliance consisted of a steel cage, a concave plate, a metal/steel mesh and a metal/steel biomass holder. The details of the combustion setup and the specific biomass holders used for each fuel type are illustrated in Supplementary Fig. S2. Combustion was initiated using an electric resistor of which the power was adjusted to generate exclusively flaming or smouldering emissions, similar to previous studies (Pokhrel et al., 2021; McRee et al., 2025). With this open combustion setup (Fig. S2), we allowed instant dilution of the emissions in an aim to simulate real world forest surface fires. Eight different types of biomasses were used as fuel samples in the combustion experiments. Namely, commercially available peat samples (CP), Finnish boreal forest surface (BFS, including vegetation, litter, and the soil organic layer), peat from two Finnish boreal peatlands (FIA and FIB), peat from arctic permafrost regions of Russia (RUS) and Norway (NOR), savanna wood and grass from South Africa (SW and SG respectively) were selected as fuels for this study. The origins and properties of the combusted biomasses are available in the Supplementary Information (Section S1, Table S1). The savanna biomass included in this study was part of the BASFAA (Boreal and savanna fire aerosol aging) measurement campaign that took place from May to June 2022 at the ILMARI laboratory as described in Vakkari et al. (2025). For this study specific combustion phases were selected for sampling representing either solely flaming, pre-flame smouldering, or full combustion consisting of pre-flame smouldering, flaming and postflame smouldering periods. Therefore, a subset of Savanna biomass (SG and SW) combustions presented in Vakkari et al. (2025), which included sampling of separate combustion phases (either flaming or pre or post

flame smouldering), were chosen to be included in this study. The sampling periods were selected based on careful visual inspection of the combustion process and the concentrations of CO and CO₂, monitored online as described below (Section 2.2).

2.2. Sampling setup and gas phase measurements

The emitted smoke was sampled using the setup presented in Fig. 1. We measured the gaseous

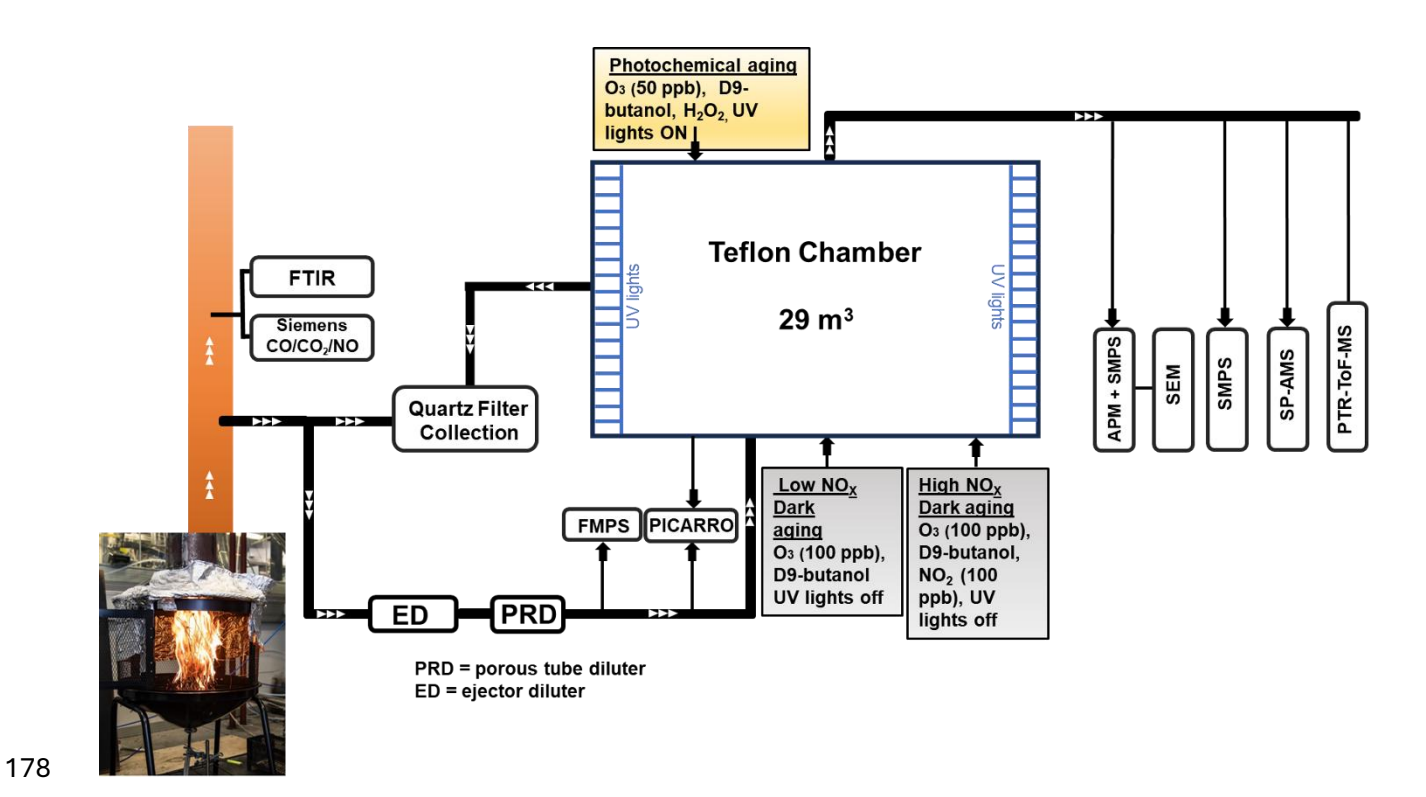


Figure 1: A schematic presentation of the experimental setup for combustion experiments involving the environmental chamber

compounds from the fresh, undiluted BB emission using an online multicomponent FTIR analyzer (Gasmet Technologies Inc.), and the measured compounds are listed in Table S2. The fresh BB emissions were sampled through a PM₁₀ pre-cyclone and a heated probe (180 °C) before being diluted using an Ejector Dilutor (Titta et al., 2016) and porous tube dilutor. A dilution ratio (DR) of 4-20 was achieved during this two-stage dilution with clean synthetic air (Woikoski N50) in ambient temperature. A gas concentration

analyzer (Picarro G2401) measured the concentrations of CO₂, CO, CH₄ and water vapor (H₂O) from the
 diluted exhaust (Fig. 1).

MCEs were calculated from the average increase in CO₂ and CO concentrations during the sampled combustion period relative to the background concentrations (Eq. 1)

$$191 MCE = \frac{\Delta[CO_2]}{\Delta[CO_2] + \Delta[CO]} (1)$$

MCE was estimated from CO and CO₂ concentrations measured in both undiluted and diluted BB emission.

Burns with average MCE values smaller than 0.9 were defined as smouldering-dominated combustion, while the combustions with average MCE values larger than 0.9 (Table 1) were classified as flaming dominated (Yokelson et al., 1996; Stockwell et al., 2014).

2.3 Environmental chamber and aging of the emissions

Different burning phases of Finnish BFS, and Finnish commercial peat (CP) samples were used in the chamber experiments to study the effects of dilution and oxidative aging on the organic aerosol optical properties. Additionally, samples of Savanna burning chamber experiments, described by Vakkari et al. (2025), were analyzed as part of this study. For peatland samples FIA, FIB, NOR and RUS, only fresh emissions were characterized in this study and no chamber feeding was performed. In each of the chamber experiments, diluted primary BB emissions were sampled into a 29 m³ Teflon™ chamber (Leskinen et al., 2015) which was pre-filled with purified air (Model 737-250, Aadco Instruments Inc.). For each experiment, the sampling period to the environmental chamber was set based on the targeted mass concentration of 20-50 μg mr³ as estimated from the fresh particle size distribution measured online by a fast mobility particle sizer (FMPS, model 3091, TSI Inc.). The relative humidity (RH) inside the chamber was set at 20% for SG and SW emissions and at around 50% for BFS and CP emissions to reproduce typical daytime RH in corresponding environments during the fire active seasons, using a humidification setup described in Leskinen et al. (2015). The temperature in the chamber was kept constant at approximately 22°C. The sample was first allowed to mix and homogenise for 20 minutes, which was an adequate duration for the mass concentrations of particulate matter (PM) and organics inside the chamber to stabilize, as observed

respectively by a scanning mobility particle sizer (SMPS) and a soot particle aerosol mass spectrometer (SP-AMS, Aerodyne Research Inc, USA) connected to the chamber. After sampling of the fresh exhaust, Picarro was switched to monitor the gaseous components inside the chamber. Total DRs inside the chamber were 135-4045 compared to the two-stage diluted fresh emission (Table 1), based on the ratio of CO concentration measured by Picarro in the diluted exhaust and from the chamber.

213

214

215

216

217

218

219

220

221

222

223

224

225

226

227

228

229

230

231

232

233

234

235

236

237

238

239

After the stabilization period, chamber diluted primary BB emissions were monitored for additional 45 mins before adding reactants to the chamber to induce oxidative aging. Oxidative reactants were injected into the chamber after the BB emissions, because we first wanted to measure the characteristics of primary aerosols as well as, to study the effect of dilution on the partitioning of the POA fraction without inducing any aging pathways, similar to previous studies (Kodros et al., 2020, 2022). The oxidative reactants were allowed to interact with the fresh BB emission in the chamber for 4.5 hours. For each experiment, 2 µL of d9-butanol (~25 ppb) was injected into the chamber and the concentration was probed throughout the experimental duration using a proton-transfer-reaction time-of-flight mass spectrometer (PTR-ToF-MS). Four distinct aging conditions were simulated in the environmental chamber to evaluate the impact of aging on the physio-chemical and optical properties of different BB emissions. Firstly, photochemical aging conditions were induced inside the chamber for both flaming and smouldering combustion. In the photochemical experiments, UV-light in presence of externally fed O₃ (50 ppb) and H₂O₂ (0.5 ml of 30% v/v solution) led to the formation of hydroxyl radicals (OH·). The OH exposure and equivalent photochemical age were determined from the decay of d9-butanol (Barmet et al., 2012). In our experiments, equivalent photochemical age ranged between 1-1.6 days (Table 1) with an assumed ambient OH concentration of 1.5×10⁶ cm⁻³. In addition, two different dark aging conditions were simulated for two distinct sets of biomasses. The primary emissions from SG and SW underwent dark aging in the presence of externally added 100 ppb of O_3 and no additional NO_x . We classified this aging condition as "low-NO_x dark aging", as the nitrate radical (NO₃) formation was limited by the lack of NO_x. CP and BFS burning emissions were aged in relatively 'high-NO_x' conditions in the dark chamber with 100 ppb NO₂ followed by 100 ppb O₃ directly injected to chamber. It should be clarified that even though we termed this aging condition as "high- NO_x ", the NMVOC/NO_x ratio was still relatively high (Seinfield and Pandis, 2006), in the range of 4-6 in

these cases (Table 1). Furthermore, the addition of O₃ within a small span of time (~10 minutes) after the addition of NO₂ in the chamber might have led to competition between the expected NO₃ radical chemistry and ozonolysis pathways, although the reaction rates of ozonolysis are much slower than nitrate oxidation pathways. Another method for simulating aerosol aging with NO₃ radicals would be to precondition the chamber with NO₂ and O₃ before adding the BB emissions (McRee et al., 2025). However, by doing this, we would not have been able to study both fresh and oxidatively aged aerosol during the same chamber experiment. Seven additional experiments were conducted in this study without any added oxidants in the chamber to evaluate the impacts of chamber dilution, estimate wall lose and other processes on the exhaust emissions. Out of these seven experiments, three were conducted by sampling emissions from the whole combustion of BFS, while the other four experiments were constituted with distinct smouldering and flaming dominated burns of CP and BFS.

2.4 Particle size distribution, density and morphology:

The particle size distributions were measured from the environmental chamber for the whole duration of each experiment by a scanning mobility particle sizer (SMPS) consisting of a differential mobility analyzer (DMA, model 3080; TSI Inc.) and a condensation particle counter (CPC, model 3775; TSI Inc.). In addition, an aerosol particle mass analyzer (APM, model 3602; Kanomax Inc.) in tandem with another SMPS (with *DMA 3081* and *CPC 3750*, TSI Inc.) was used to measure the size distribution of mass classified particles to estimate the size-resolved effective densities of the particles (Leskinen et al., 2023; Mukherjee et al., 2024). Particle densities of primary emission from the chamber were measured before the application of any additional reactants to the chamber. The density of the aged particles in the chamber were measured 4.5 hours after the addition and stabilization of the reactants (for dark aging) and/or turning on of the UV lights (for photochemical aging; Table S4). Simultaneous to the density measurements, particles were collected on holey-carbon grids (S147-4 Holey carbon film 400 Mesh Cu; Agar Scientific Inc.) from the chamber using an aspiration sampler at a flowrate of 0.3 litres per minute (lpm). Subsequently, we performed Scanning Electron Microscopy (SEM, Sigma HD/VP; Carl Zeiss NTS) to investigate the morphology of both chamber diluted primary and aged BB emitted particles.

2.5 Offline optical analyses:

Biomass burning emissions were collected on precombusted 90 mm Quartz microfiber filter (PallflexTM TissuguartzTM 7203, Pall Corporation) from the fresh emissions and at the end of each chamber experiment. First, the freshly emitted particles from the raw exhaust without any additional dilution were deposited on the filter at a flow rate of 90 lpm. For experiments with subsequent chamber study, the sampling was done for the same duration as the chamber feed (Fig. 1). Approximately 4.5 hours after the chamber feeding, another filter sample was collected from the chamber with the same flow rate for 120 minutes. For the boreal (FIA and FIB) and arctic peat (RUS and NOR) samples, the primary emission was deposited on the filter throughout the whole combustion period, and no chamber studies were performed. Thermal-optical carbon analysis was carried out with the IMPROVE-A protocol (Chow et al., 2007) in a carbon analyzer (Lab OC-EC Aerosol Analyzer; Sunset Laboratory Inc.) by placing 1.5 cm² punches of the Quartz fiber filters (QMA) containing deposited aerosol particles. The details of the measurement protocol have been described in the supporting information (Section S2). Additionally, two separate 1.5 cm² filter punches from each experiment were extracted, one with ultrapure Mili-Q water (>18.2 MΩ) and the other with MeOH (Fisher Scientific, Analytical Reagent Grade >=99.9% pure). After solvent extraction, the two filters were dried under gentle airflow in a clean room for 12 hours before being analysed with the same OC-EC analyzer. This setup (Fig. S4) enabled us to measure the dissolved organic concentration in the solvent using Eq. 4 (see section 2.8) and therefore estimate the MAE_{OC} (Eq. 3).

267

268

269

270

271

272

273

274

275

276

277

278

279

280

281

282

283

Table 1: List of chamber experiments with detailed parameterization of combustion and aging conditions (mean ± standard deviation)

No.	Fuel	Combustion	MCE	OC EF (fresh	EC EF (fresh	Final DR	SMPS PM ₁ EF (g	GMD	Aging condition	NMVOC/NO _x	OH exposure	eqv. age
		Condition		emission)	emission)	(chamber)	kg ⁻¹) (chamber	(nm)	(in chamber)	(ppbC/ppb)	(x 10 ¹¹ molecules.cm ⁻³ . s ⁻¹)	(days)
		(no. of replicates)		(g kg ⁻¹)	(g kg ⁻¹)		primary)					
1a	CP	flaming (n = 2)	0.971 ± 0.004	5.34 ± 2.32	0.29 ± 0.08	247 ± 106	6.98 ± 4.01	52.4 ± 1.60	photo aged	21.4 ± 4.40	2.09 (± 0.33)	1.61 ± 0.26
1b		flaming (n = 1)	0.979	1.85	0.40	229	3.86	48.0	high NO _x dark aged	5.45	NA	
1c		flaming (n = 1)	0.986	1.39	1.81	273	8.05	54.4	no aging	6.40	NA	
1d		smouldering (n = 2)	0.619 ± 0.147	58.3 ± 31.5	0.24 ± 0.07	764 ± 118	152 ± 89	48.3 ± 5.20	photo aged	88.6 ± 5.01	1.15 (± 0.63)	0.88 ± 0.48
1e		smouldering (n = 1)	0.793	26.8	0.16	429	33.6	45.5	high NO _x dark aged	4.20	NA	
1f		smouldering (n = 1)	0.479	73.7	0.49	666	228	59.7	no aging	108	NA	
2a	BFS	flaming (n = 3)	0.922 ± 0.003	3.20 ± 0.94	0.43 ± 0.15	309 ± 199	6.07 ± 1.05	51.0 ± 4.10	photo aged	63.9 ± 41.7	1.80 (± 0.34)	1.39 ± 0.26
2b		flaming (n = 3)	0.952 ± 0.005	3.18 ± 0.70	0.39 ± 0.08	387 ± 140	4.79 ± 0.82	51.6 ± 0.70	high NO _x dark aged	4.78 ± 1.23	NA	
2c		flaming (n = 1)	0.961	3.06	0.73	833	5.95	53.6	no aging	20.0	NA	
2d		smouldering (n = 3)	0.759 ± 0.020	23.9 ± 15.7	0.08 ± 0.07	276 ± 100	48.3 ± 29.5	84.7 ± 41.4	photo aged	133 ± 104	1.57 (± 0.11)	1.21 ± 0.09
2e		smouldering (n = 3)	0.761 ± 0.017	24.0 ± 10.5	0.07 ± 0.06	287 ± 123	26.6 ± 21.1	73.2 ± 22.8	high NO _x dark aged	23.5 ± 19.6	NA	
2f		smouldering (n = 1)	0.774	15.3	0.33	135	23.96	51.2	no aging	163	NA	
3a	SW	flaming (n = 1)	0.935	8.04	0.97	922	12.4	60.5	photo aged	26.1	1.41	1.09
3b		flaming (n = 1)	0.950	5.93	0.60	244	10.5	48.0	low NO _x dark aged	43.9	NA	
3c		smouldering (n = 1)	0.589	87.0	5.18	389	61.1	81.0	photo aged	53.2	1.29	0.99
3d		smouldering (n = 1)	0.892	22.5	1.36	416	31.1	62.6	low NO _x dark aged	69.7	NA	
4a	SG	flaming (n = 1)	0.943	4.83	0.31	512	6.24	48.1	photo aged	124	1.46	1.13
4b		flaming (n = 1)	0.973	2.87	0.28	1974	5.44	50.3	low NO _x dark aged	2.73	NA	
4c		smouldering (n = 1)	0.803	31.8	1.19	4045	28.6	60.5	photo aged	19.3	1.49	1.15
4d		smouldering (n = 1)	0.843	14.0	1.25	902	23.2	58.5	low NO _x dark aged	108	NA	

For filters containing fresh emissions collected from the raw exhaust, 40 mL of solvent was used for the extraction of the 1.5 cm² filter area. The volume of solvent used for extraction of highly loaded filters containing fresh emissions can be a limiting factor for dissolved OC concentration, especially for BB emitted particles that have been shown to be dominated by non-polar molecules (Lin et al., 2017) that are less soluble in water. We chose 40 ml of solvent, as this volume provided a dilute micromolar solution in which the light absorption by the dissolved organics would be linearly proportional to their concentration, in accordance with Beer-Lambert's law (Huang et al., 2018). The utilized solvent volume was also sufficient to dissolve the sparingly soluble low volatility strongly light-absorbing fraction of OC. On the other hand, for the chamber diluted fresh emissions and aged particles, two 1.5 cm² filter punches (total of 3 cm²) were extracted in 20 mL water or MeOH (Cao et al., 2021; Fan et al., 2018) to obtain solution phase organic concentrations necessary for analytically significant S/N ratio in the UV-vis spectrophotometry. In parallel to the deposition of primary particles from the raw exhaust on quartz fiber (QMA) filters for emission factor calculation, a fraction of the emitted particles was fed to the TeflonTM chamber to create real life atmospheric dilution. It is important to study these particles in a diluted system to understand their chemical and optical evolution in the atmosphere. The particle size distribution, effective density, and morphology of the primary BB emission were studied after feeding them in the chamber and letting them mix homogeneously with clean air. Subsequently, different oxidants were added to the chamber to initiate photochemical or dark oxidation reactions. After 4.5 hours of feeding the oxidants, the particles from the chamber were deposited on another QMA filter. In addition to that, five separate experiments were conducted for different BB emissions, where no oxidants were directly injected to the chamber and the primary particles were on QMA filter 4.5 hours after the chamber feed. These samples are referred to as "chamber primary" samples. The QMA filters containing chamber aged and chamber primary particles were produced to undergo OC-EC analyses and solvent extraction similar to the QMA particles collecting raw exhaust primary particles. The filter punches were submerged in the solvents and sonicated for 10 mins in three separate intervals in an optimized ultrasonicator (SONOREX Digitec, Bandelin Inc.). The optimization enabled a much gentler

286

287

288

289

290

291

292

293

294

295

296

297

298

299

300

301

302

303

304

305

306

307

308

309

310

311

312

sonication as compared to regular commercial ultrasonicators (Huang et al., 2018; Li et al., 2020), resulting

in high extraction efficiencies without damaging the filter punch and thereby allowing subsequent OC-EC analyses. Such gentle ultrasonication also minimised the dislodging of insoluble organics or EC from the filter to the solution (Phillips and Smith, 2017). During the intervals between the 10-minute sonication windows, the samples were kept in a refrigerator to keep the effects of any thermal disintegration of OC or chemical transformation through reactions with the solvent (Bateman et al., 2008; Chen et al., 2022) due to the added kinetic and thermal energy during the sonication at minimal.

After the sonication, the elute was passed through 0.2 um hydrophilic PTFE syringe filters (Fisherbrand) to remove any insoluble particles from the solution. Aliquots of 3 mL from the filtered solutions were taken in a quartz cuvette with 1 cm path length and UV-vis spectra were recorded for the wavelength range of 250-700 mm using a spectrophotometer (UV-2401 PC, Shimadzu). The overall contact time between the solvent and the extracted organics in the solution never exceeded 2 hours before the recording of the optical spectra.

These were much smaller time intervals compared to the reaction rates between MeOH and carboxyl groups for instance (McIntyre and McRae, 2005), enabling us to disregard any potential artifact caused by the

solvent (MeOH) to the chemical composition of the original OC deposited on the filter (Lin et al., 2012).

2.6. Residential wood combustion experiments

In addition to different open BB emissions, filter samples from experiments performed with modern European logwood-fired chimney stove (Aduro 9-3) operated with beech logs from two separate experimental campaigns were included in the study. This enabled us to extend the analysed sample set to conditions representing high-temperature biomass combustion, and to test the validity of the BrC-BC continuum. The general experimental setups of these two sets of experiments have been presented in our previous works (Ihalainen et al., 2019a, Mukherjee et al., 2024). Each experiment consisted of four (Ihalainen et al., 2019a) or six (Mukherjee et al., 2024) 45 min batches of wood log burning, ignited with wood sticks as kindling. Photochemical aging of the residential wood combustion (RWC) exhaust was conducted by the Photochemical Emission Aging flow tube reactor (PEAR, Ihalainen et al., 2019b), in similar conditions as the low-dilution aging in Hartikainen et al. (2020). Briefly, exhaust samples were collected onto quartz fiber filters before and after the PEAR in a flow rate of 10 lpm for 60 min, with each sample consisting of one full batch and 20 min of the subsequent batch, either from the cold stove (consisting

- of 1st and 2nd batch of wood) or in the warm stove (consisting of 3rd and 4th batches of wood) combustion.
- 341 The filter samples were extracted similarly to the open biomass burning samples for optical analyses.

342 2.7. Optical data processing:

- 343 The raw absorption (A) of the extracted solution measured by the UV-vis spectrophotometer was converted
- to the light absorption coefficient (β_{abs} , Mm⁻¹) in the sampled air using Eq. 2 (Hecobian et al., 2010):

345
$$\beta_{abs}(\lambda) = \frac{(A_{\lambda} - A_{700}) \times V_l \times \ln(10)}{V_a \times l}$$
 (2)

- where A_{λ} is the raw absorbance measured by the spectrophotometer in base-10 at wavelength λ and A_{700} is
- 347 the absorption at 700nm (which was subtracted from A_{λ} to correct for baseline drift caused by the
- absorption), V_l is the volume of the extract, V_a (m³) is the volume of the air sampled through the quartz filter
- during emission measurements, l is the path length of light through the solution, which is equivalent to the
- width of the quartz cuvette (0.01 m).:
- The mass absorption efficiency (MAE) of the extracted BrC at a particular wavelength λ is given by Eq. 3
- 352 (Liu et al., 2013):

353
$$MAE(\lambda) = \frac{\beta_{abs}(\lambda)}{c}$$
 (3)

- 354 where C is the concentration of the dissolved organic in a particular solvent (g m⁻³). C for MeOH and water
- soluble organics (C_{MSOC} and C_{WSOC} respectively) were calculated as:

$$C_{MSOC} = \frac{\text{(OC in original filter)} - \text{(OC in MeOH extracted filter)}}{volume \ of \ methanol \ used \ for \ extraction}$$
(4a)

358 and,

356

360

362

363

$$C_{WSOC} = \frac{(\text{OC in original filter}) - (\text{OC in water extracted filter})}{volume \ of \ water \ used \ for \ extraction}$$
 (4b)

361 C_{WSOC} was also directly measured from the aqueous filter extracts using a total organic carbon (TOC/TN)

analyzer (TOC-L, Shimadzu) to compare with the estimates obtained using Eq. 4b. Overall the two methods

yielded comparable C_{WSOC} values ($R^2 = 0.98$, Fig. S5,), so for consistency we have used the filter based C

values for both MSOC and WSOC in calculating MAE. The solubility of organics in each solvent were estimated as:

solubility =
$$\frac{\text{(OC in original filter)} - \text{(OC in extracted filter)}}{\text{(OC in original filter)}}$$
(5)

The imaginary part of the refractive index, k, was related to MAE at any given wavelength λ according to
 Jennings et al. (1979):

369
$$MAE(\lambda) = \frac{4\pi k(\lambda)}{\rho \lambda}$$
 (6)

where ρ is the density of the dissolved organic (g cm⁻³). For fresh, photochemically aged and dark aged emissions different mean density values were used for calculating k as mentioned in Table S4. For the RWC experiments, particle densities measured for fresh and PEAR-aged beech combustion exhaust particles from the same appliance (Mukherjee et al., 2024). were applied for the calculation of k. Specifically, density values of $1(\pm 0.1)$ g cm⁻³ and $1.6(\pm 0.1)$ g cm⁻³ were used for the primary and aged RWC exhaust particles, respectively. It should be noted that the MAE values obtained in this study for soluble OC will need to be divided by an OA/OC factor (typically in the range of 1.8-2.2 for fresh emissions, Hartikainen et al., 2020) to obtain the MAE of MeOH or water-soluble OA before comparing with previous literature reporting light absorption properties of BB emitted OA.

Absorption Ångström exponent (AAE) of MSOC and WSOC were estimated between a pair of wavelengths
 λ₁ and λ₂ as the power law exponent of the ratio between the absorption coefficients at the two wavelengths
 (Moosmüller et al., 2009), such as:

383
$$AAE(\lambda 1, \lambda 2) = \frac{\ln\{\beta_{abs}(\lambda 1)/\beta_{abs}(\lambda 2)\}}{\ln(\lambda 2/\lambda 1)}$$
 (7)

For this study, AAE between wavelengths 300-550 nm were used to describe the optical behaviour of BrC emitted from different biomass sources. The wavelength dependence of the imaginary refractive index k is denoted as w (Saleh et al., 2014) which we derived for fresh and chamber samples using a similar power law relationship as Eq. 7 but involving k at two different wavelengths. In literature, w has also been estimated using AAE (Saleh et al., 2014, McClure et al., 2020) as they are related by:

389
$$AAE \approx w + 1$$
 (8)

390 2.8 Emission Factor Calculation

- 391 Emission factors from the combustion experiments were calculated by the carbon mass balance method such
- 392 (Eq. 9; Yokelson et al., 1999)

393
$$EF_X = F_C \cdot 1000 \cdot \frac{ER_X}{\frac{\sum \Delta C}{\Delta CO}}$$
 (9)

- where F_c is carbon fraction in the combusted sample and the summation $\sum \Delta C$ is the total carbon released
- during the combustion. For savanna biomasses (SG and SW) $\sum \Delta C$ was estimated as (Vakkari et al., 2025):

396
$$\sum \Delta C = \Delta C O_2 + \Delta C O + \Delta C H_4 + \Delta O C + \Delta r B C + \sum \Delta C_{VOC}$$
 (10 a),

- 397 ΔCO_2 , ΔCO and ΔCH_4 were their respective concentrations in ppm subtracted by background and synthetic
- 398 air concentration, ΔOC was measured by AMS, rBC was measured by SP2 and VOCs were measured by
- 399 VOCUS. For commercial peat (CP), boreal forest surface (BFS) and natural peatland (FIA, FIB, RUS and
- 400 NOR) emissions, $\sum \Delta C$ weas estimated as:

401
$$\sum \Delta C = \Delta C O_2 + \Delta C O + \Delta C H_4 + \Delta O C + \Delta E C + \sum \Delta C_{VOC}$$
 (10 b),

- 402 For CP and BFS, CO₂, CO and CH₄ were measured using Picarro and non-methane VOCs (NMVOC) were
- 403 estimated from FTIR (Table S2). For natural peatland samples CO, CH₄ and NMVOCs were all measured by
- FTIR, while CO₂ was measured by a CO₂ analyzer (Siemens). OC and EC for all of these samples were
- 405 estimated from OC-EC analyses of filters.
- 406 ER_x in Eq. 9 is the ratio of measured concentration in $\mu g \ m^{-3}$ relative to the CO carbon concentration in
- 407 μgC m⁻³. ER_x was calculated by Eq. 11, where the CO concentration measured in ppm is converted to CO
- 408 carbon concentration in μ gC m⁻³ using the following equation:

409
$$\Delta ER_X = \frac{X}{\frac{12.01 \, g/mol * 101325 \, Pa}{8.31451 \, J/mol \cdot K * (295.15 \, K + T)} x \Delta CO}$$
(11)

- Where X is the concentration of the measured parameter in μ g m⁻³, Δ CO is the CO concentration in the
- emission in ppm compared to background, T is measured temperature in the chamber in Kelvin (295.15 K or

22°C), 12.01 is the molecular weight of carbon (g mol⁻¹), 101325 standard atmospheric pressure in Pa,

8.31451 is gas constant in SI unit.

2.9 FT-ICR MS analyses:

412

413

414

415

416

417

418

419

420

421

422

423

424

425

426

427

428

429

430

431

432

433

434

435

436

437

Chemical compositions of the biomass burning emission samples collected on quartz filters were characterized by means of ultrahigh-resolution mass spectrometry. All experiments were performed using a 12-T Bruker solariX XR Fourier transform ion cyclotron resonance mass spectrometer (FT-ICR MS) (Bruker Daltonics GmbH, Bremen, Germany), equipped with a dynamically harmonized ICR cell (ParaCell®). The mass spectrometer was coupled to an Apollo-II atmospheric pressure chemical ionization (APCI) source, fitted with a direct insertion probe (DIP) accessory. This set-up enabled chemical characterization of the filter samples directly with minimal sample preparation. Five layers of each quartz filter sample were packed into a prebaked glass capillary (Hirschmann melting point tube) and inserted into the ion source vaporizer, held at 370 °C. The capillary voltage was set to 4500 V and corona current to 4000 nA. Dry nitrogen was used as the drying (3.5 Lmin⁻¹, 220 °C) and nebulizing (2.0 bar) gas. After an induction time of 10 s, the MS data were recorded until the total ion current plateaued (i.e number of scans ranged from 15 to 35), indicating that the entire aerosol sample was completely desorbed at the given temperature. All DIP-APCI FT-ICR measurements were conducted in a positive ion mode. The generated ions were accumulated in the hexapole ion trap and transferred to the ICR cell for trapping, excitation and detection. The instrument control and data acquisition were performed by Bruker ftmsControl 2.1 software. For each spectrum, a broadband frequency excitation and detection were carried out with 4 MWord time-domain transients (transient time 1.1 s), which were full-sine apodized and zero-filled once to provide the final 8 MWord magnitude-mode data spanning m/z range of 100–2000. The time-of-flight and ion accumulation time settings were 1.0 ms and 0.30 s, respectively. The FT-ICR instrument was externally m/z-calibrated prior to the measurements using a polystyrene (PS) standard covering a wide mass range and reaching accuracies generally below 1 ppm. The initial spectral post-processing was done with Bruker DataAnalysis 5.1 software, including the internal re-calibration of the m/z-axes with a custom-made mass list for organic aerosol samples. For the peak picking, a signal-to-noise

(S/N) ratio was set at ≥6. PetroOrg IS 18.0.3 software (Omics LLC, Tallahassee, FL, USA) was used for the molecular formula assignments with the following constraints: double bond equivalent (DBE) 0–40; mass error ±1.0 ppm; atomic formula ¹²C₁₋₁₀₀¹H₁₋₂₀₀¹⁴N₁₋₄¹⁶O₁₋₁₅³²S₁₋₄. The elemental composition boundaries for the annotation were chosen based on careful manual inspection of spectra identifying the edges of the observed chemical space. The time-resolved spectral information of the DIP experiment had been summed to an average spectral read back for each measurement.

For data interpretation and visualization of the complex lists of attributed sum formulae, we used established data grouping and fingerprint diagrams (Schneider et al., 2024a; 2024b). Visualization and pre-processing, calculating molecular properties and diagnostic measures from the sum formulae were performed via MATLAB (MATLAB R2023a, MathWorks Inc., MA). Characteristic molecular properties encompassed double bond equivalents (DBE), aromaticity index (AI), saturation vapor pressure (C*) and average carbon oxidation state (OS_C) frequently used in ultra-high resolution mass spectrometric studies of complex environmental sample materials (Koch and Dittmar, 2006; Kroll et al., 2011; Li et al., 2016)

2.10: SP-AMS analyses:

This study employed a soot particle aerosol mass spectrometer (SP-AMS; Aerodyne Research Inc., Billerica, MA, USA; Onasch et al., 2012) to analyze the concentration levels, mass spectral signatures, and size distributions of non-refractory (organics, sulfate, nitrate, ammonium, and chloride) and refractory (e.g. metals, rBC) components. The SP-AMS enhances the capabilities of the standard AMS by incorporating a laser vaporizer, which enables the analysis of refractory aerosol components. While the instrument can function using only the laser vaporizer, both the laser and tungsten vaporizers were used in this study to ensure comprehensive detection of mentioned chemical species. Size-resolved measurements were obtained using particle time-of-flight (PToF) mode, with the SP-AMS aerodynamic lens enabling detection of particles ranging from roughly 50 nm to 1 μm. The instrument operated with a time resolution of 60 seconds, with about half of the time measuring in mass spectrum mode and the other half in PToF mode. A calibration of the SP-AMS based on particle mass was carried out using size-selected, dried particles of ammonium nitrate and ammonium sulfate. This approach allowed for the determination of an effective nitrate response factor, as well as the relative ionization efficiencies (RIES) for ammonium (RIENH4) and sulfate (RIESO4).

by converting the instrument signals into nitrate-equivalent mass concentrations. The determined RIE value for NH4 was 3.4 while the one for sulfate was 0.9. A default RIE value of 1.4 was used for organics. SP-AMS data processing was conducted using the AMS analysis tools SQUIRREL (version 1.63B) and PIKA (version 1.23B) within Igor Pro 8 (Wavemetrics, Lake Oswego, OR).

469

470

471

472

473

474

475

476

477

478

479

480

481

482

483

484

485

486

487

488

489

490

465

466

467

468

3. Results

3.1 Emission factors of OC and EC in fresh emission

The emission factors of OC (EF_{OC}) and EC (EF_{EC}) were determined based on thermal-optical carbon analyses of filters collected from fresh exhaust aerosol (Fig. 2, Fig. S6). Generally, we observed higher EF_{OC} for smouldering combustions with low MCE, as expected. For EC however, the trend was reversed, with flaming combustion having higher MCE producing more EC per kg of fuel (Fig. S6). The combustion emissions in our experiments were OC rich, most likely due to the open setup of the burner, which resulted in lower combustion temperature compared to wood stove emissions, due to high air-to-fuel ratios and because there is no combustion chamber around the fire to retain the heat in the surroundings. However, there were significant variations in EF_{OC} obtained from different combustion conditions and for different biomasses, ranging from 1.39-7.44 g kg⁻¹ for flaming dominated combustions and 6.12-89.9 g kg⁻¹ for smouldering dominated combustions. CP and SW samples had the largest EF_{OC} of 53.4(±29.0) g kg⁻¹ and 50.6(±29.8) g kg⁻¹ respectively, during the smouldering combustion phase. In contrast, full combustion of different natural peat samples yielded EF_{OC} in the range of 5.06-32.7 g kg⁻¹, with FIA (at depth of 30-60 cm) having the smallest (6.09±1.2 g kg⁻¹) and FIB (at depth of 30-60 cm) having the largest (29.8±2.92 g kg⁻¹) average EF_{OC} among peat samples. Interestingly, the average MCE values and EF_{OC} reported for field measurements of subtropical Indonesian peat fires (Stockwell et al., 2015; Jayarathne et al., 2018) and laboratory studies of North American (Black et al., 2016; Chakrabarty et al., 2016), West European (Iinuma et al., 2007) and South-east Asian peat fires (Christian et al., 2003; Iinuma et al., 2007) fell inside the range of our reported EF_{OC} for laboratory combustion of Finnish (boreal) and arctic peat samples. In our study, flaming and smouldering combustion of BFS samples had average EF_{OC} of 3.17(±0.77) g kg⁻¹ and

 $21.5(\pm 13.8)$ g kg⁻¹ respectively, while previously reported EF_{OC} for North American boreal forest fires were in similar range of $5.9(\pm 2.5)$ g kg⁻¹ (Andreae, 2019). Savanna wood and grass (SW and SG) samples burnt under flaming conditions in this study were estimated to have average EF_{OC} of $6.47(\pm 0.98)$ g kg⁻¹ and $3.56(\pm 0.91)$ g kg⁻¹ respectively, which were somewhat higher in comparison to previously reported organic emission factor of $3.0(\pm 1.5)$ g kg⁻¹ (Andreae, 2019) and $2.62(\pm 1.24)$ g kg⁻¹ (Akagi et al., 2011) from high MCE savanna fires.

491

492

493

494

495

496

497

498

499

500

501

502

503

504

505

506

507

508

509

510

511

512

513

514

515

516

517

Emissions from savanna biomass had higher average EF_{EC} compared to the other biomasses, with an average EF_{EC} of 3.03(±1.77) g kg⁻¹ and 0.94(±0.16) g kg⁻¹ from the smouldering emissions of the woody (SW) and grassy (SG) fuels respectively. The carbonaceous fraction of flaming dominated emissions from the woody savanna samples (MCE $\sim 0.94\pm 0.01$) consisted of 12(± 2) % of EC while savanna grass had an EC content of 7.4(±1.5)% (MCE ~0.96±0.01). Previously reported average EF_{EC} values for savanna and grassland fires ranged from $0.37(\pm 0.20 \text{ g kg}^{-1})$ (Akagi et al., 2011) to $0.53(\pm 0.35)$ g kg⁻¹ (Andreae, 2019) while Vakkari et al. (2018) reported EF_{EC} of 0.67 g kg⁻¹ for South African savanna grass burning. These values fell in between our estimated EF_{EC} from flaming burn of savanna grass (0.27±0.01 g kg⁻¹) and wood (0.72±0.17 g kg⁻¹). Full combustion (MCE 0.74-0.89) of the Finnish peat samples (FIA and FIB) collected at the depth of 30-60 cm from the surface level and arctic permafrost peat samples from Svalbard (NOR) and Russia (RUS) had the lowest measured average EF_{EC} (in the range of 0.02-0.13 g kg⁻¹), which matched well with previously reported EF_{EC} from field and lab studies of subtropical Indonesian (Stockwell et al., 2015; Christian et al., 2003) and laboratory replicates of North American peat fires (Black et al., 2016). Flaming and smouldering combustions of CP had average EF_{EC} of 0.70(\pm 0.65) g kg⁻¹ and 0.28(\pm 0.14) which resembled EF_{EC} reported from laboratory studies of Western European and South-East Asian peat fires (Iinuma et al., 2007). Burning of the boreal forest surface sample (BFS) resulted in higher EC emissions than any of the peat samples with an average EF_{EC} of 0.45(±0.16) g kg⁻¹ for high MCE (~0.94±0.01) combustion and an average EF_{EC} of 0.11(±0.09) g kg⁻¹ for low MCE (~0.76±0.02) smouldering burns. For North American boreal forest fires, Andreae (2019) reported EF_{EC} of 0.43(±0.21) g kg⁻¹ with the fire having an average MCE of 0.89(±0.04), which resembles Finnish BFS EF_{EC} for flaming dominated burns. Thus, it seems that our experiments with simulated surface fire conditions at comparably lower combustion

temperature typical for Eurasian wildfires yield similar EC emissions as reported for North American wildfires that are commonly high temperature crown fires. The estimated EC/OC ratios for fresh BB emissions in this study ranged between 0.003-1.3, which roughly corresponds to BC/OA range of 0.002-0.7, with the lowest values obtained during smouldering and higher values during flaming dominated emissions respectively.

In comparison, for residential wood combustion (RWC) of North European beech wood logs (Mukherjee et al., 2024) the respective average OC and EC emission factors were $0.64(\pm0.31)$ g kg⁻¹ and $0.28(\pm0.04)$ g kg⁻¹, respectively. Therefore, the OC emission factors for the open burning in the current study were approximately 4-140 times higher for smouldering emissions and 2-13 times higher for flaming emissions than our previous estimates of RWC emission. In comparison, we did not observe such a significant difference between the EC emission factors of RWC and flaming BB emissions. This implies that surface fires have the potential to be important sources of specifically organic pollutants and BrC in forest fire prone environments, whereas the BC emissions would not be particularly strong from these fires.

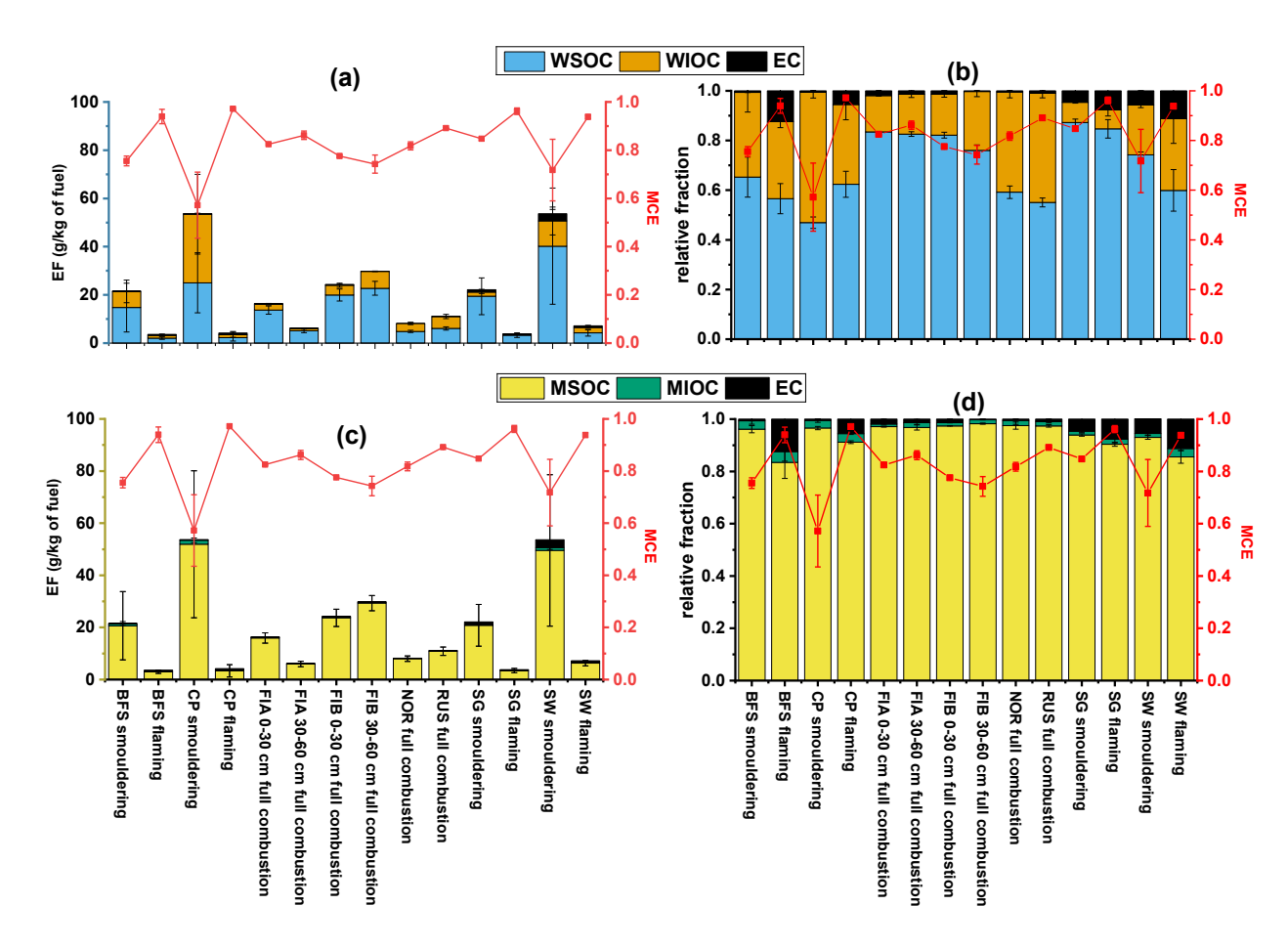


Figure 2. Emission factors of water-soluble (WSOC), MeOH soluble (MSOC), water-insoluble (WIOC), MeOH insoluble organic carbon (MIOC) and elemental carbon (EC) in absolute scale (a,c) and relative to total EF (b,d).

3.2 Chemical composition and solubility of fresh organic aerosol

532

533

534

535

536

537

538

539

540

541

542

543

544

545

546

547

548

549

550

551

552

553

554

555

556

557

558

559

Chemical characterization of the fresh emission samples from whole combustions of peat (FIA, FIB, RUS and NOR) and Finnish BFS have been previously reported by Schneider et al. (2024a) in which electrospray ionization (ESI) was utilized for the FT-ICR mass spectrometry on extracts, targeting the polar constituents. For this study, the filters containing specifically flaming and smouldering emissions of CP and BFS were analyzed directly from the filters by using 12-T DIP-APCI FTICR-MS to identify differences in the organic matter compositions due to both fuel and combustion conditions. The advantage of the DIP-APCI technique used in this study is the ability to detect analytes with low solvent extraction recoveries due to minimal sample preparation required (Rüger et al., 2021). Additionally, APCI was able to address a wide chemical space covering polar up to apolar analytes. Therefore, inspite of the lower mass loadings on the filters for specific combustion phases compared to full biomass combustions as reported in Schneider et al. (2024a), we could assign up to 2000-4000 monoisotopic elemental compositions. Overall, CHO, CHNO and CH compound classes were the most abundant in the fresh BB emissions of CP and BFS. The low temperature smouldering combustions have been shown to emit mostly direct thermal degradation products from biomass pyrolysis (Chakrabarty et al., 2016) compared to flaming combustion (Engling et al., 2006, Popovicheva et al., 2019), with similar chemical composition and molecular structures to that of the fuel (Kourtchev et al., 2011). Similar to the smouldering dominated peat burning emissions reported in Schneider et al. (2024a), we also observed that the CP smouldering emissions were chemically most diverse with the highest number of sum formulae unique to this burning condition (in total 774), thus reflecting the complex inherent compositional variability of the peat samples (Figure 3). CP smouldering emissions also had clearly higher CHN and CHNO fractions than all the other biomasses and combustion conditions. This observation can be attributed to the fact that the CP samples contained only below-surface peat that have decomposed for longer time periods and experienced more microbial activity than the BFS samples, leading to higher N containing species. Flaming combustion of CP emitted the second highest number of unique sum formulae (in total 297) but had much lower CHN class content compared to smouldering conditions, suggesting a considerable effect of the burning condition / MCE on the POA chemical composition (Figure 3).

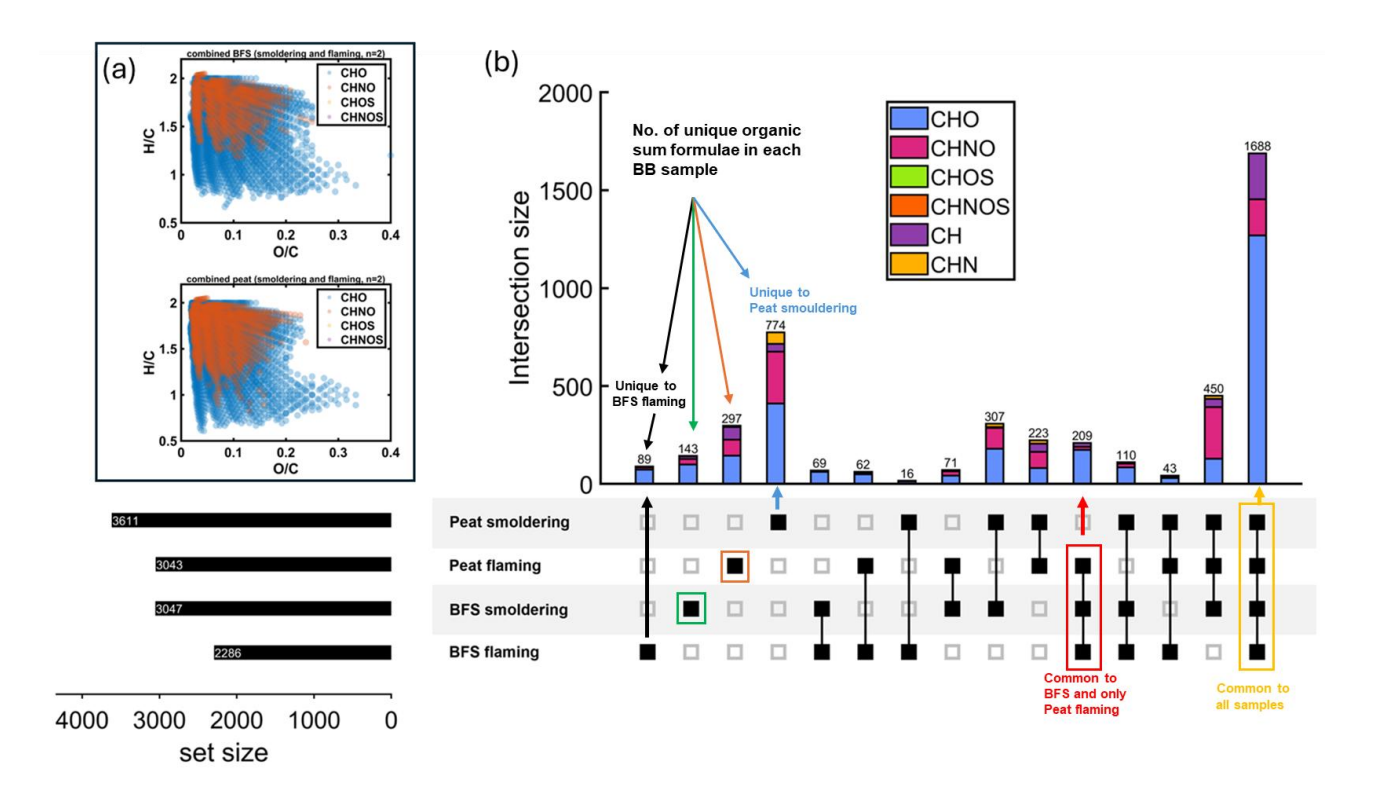


Figure 3: (a) Van-Krevelen diagrams of oxygen-containing compounds and (b) upset plot intersections (combined CP and BFS) with compound class indicated by colour. Samples were analysed by positive-ion DIP-APCI FT-ICR mass spectrometry. Upset plot of four organic aerosol datasets (flaming and smouldering emissions of CP and BFS) with the number of measured molecular formulae in each dataset (bottom left) and the individual intersections (top right) indicated by colour (CHO-light blue, CHOS-green, CH-purple, CHNO-magenta, CHNOS-orange and CHN-yellow). The compared samples are shown in the lower right corner and the common organic sum formulas they contain in the panel on the upper right.

On the other hand, the BFS smouldering and flaming emissions exhibited chemically similar compounds, with nearly 1900 identified molecular formulae shared among all the analysed BFS samples. Almost none of the molecular formulae were unique to BFS smouldering or flaming samples, as the variability among replicates themselves was high. This indicates that although different combustion conditions of BFS strongly influence the OC emission factor, it does not lead to prominent chemical differences in POA. Similar to CP, BFS emissions were also dominated by CHO, CHNO and CH classes, although a much lower fraction of CHN was present in the BFS smouldering emission compared to CP. Furthermore, a more detailed inspection of the identified formulae of the nitrogen-containing molecules in the fresh CP and BFS emissions reveals that they mostly belonged to the CHNO class, contained one nitrogen substitution, and consisted of

both aliphatic and aromatic nitro-organic compounds (Figure 4). Specifically, nitroaromatics were more abundant in the peat samples, which is relevant, as nitroaromatics are known to be prominent BrC chromophores absorbing light in the wavelength range of 360-600 nm (Fleming et al., 2020).

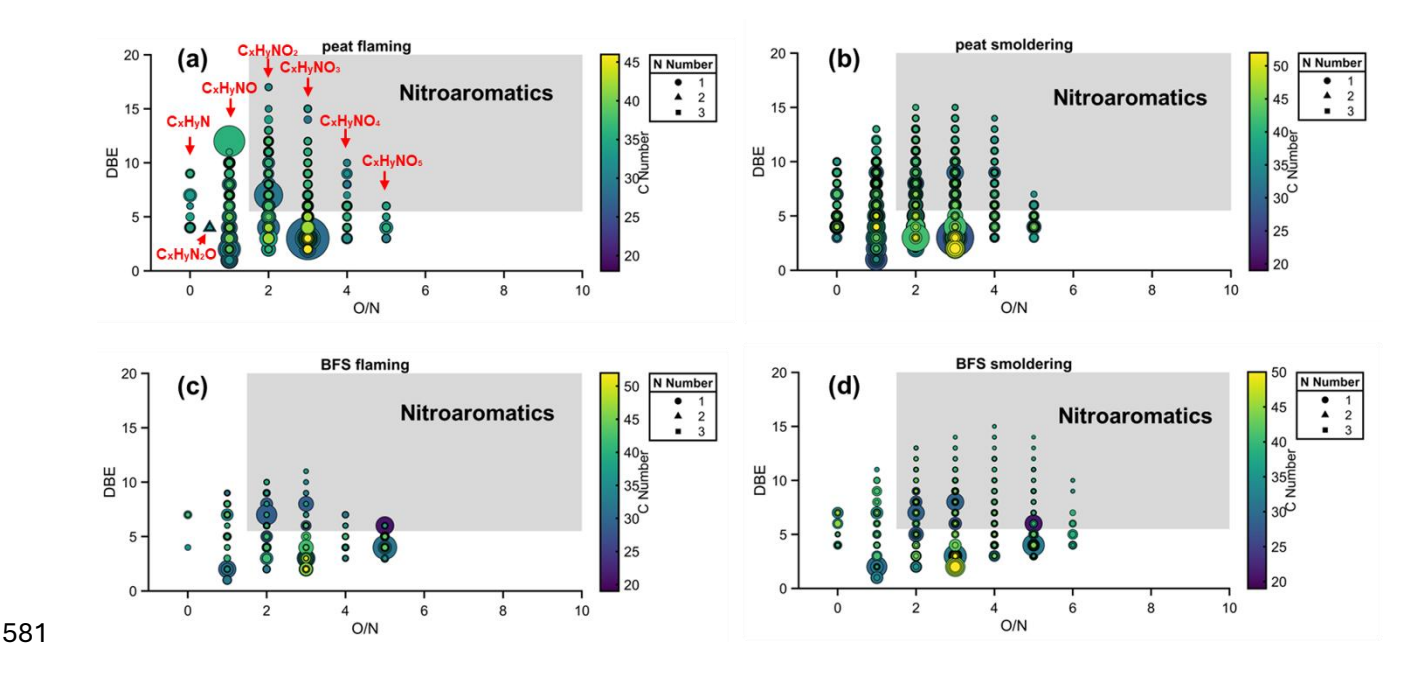


Figure 4: Detailed chemical characterization of CHN and CHNO compounds in (a) CP flaming, (b) CP smouldering, (c) BFS flaming and (d) BFS smouldering fresh emissions. The x-axis shows O:N ratio and y-axis corresponds to double-bond equivalence (DBE). Nitroaromatic compounds fall into the shaded (grey) area in the figures.

Due to their different chemical compositions, OC from various fresh BB emissions exhibited variable solubility in water and MeOH (Fig. 2, Fig. S11). While MeOH extracted almost all the OC (~95%) from the filter irrespective of fuel or combustion type, the water-soluble fraction of OC (WSOC) exhibited fuel dependent behaviour. For example, both FIA and FIB emissions exhibited higher WSOC fractions (76-83%) in the total organic carbon (TOC) compared to arctic permafrost peat samples NOR (~59% of TOC) and RUS (~55% of TOC). This has been previously elaborated by Schneider et al. (2024a), who found that in comparison to FIA and FIB samples, NOR and RUS peat combustion emissions were constituted by less oxidized primary organic carbon (POC), which explains the diminished solubility in a polar solvent like water (Budisulistiorini et al., 2017). Among the biomass samples used in this study, SG showed the highest WSOC fractions for both flaming (~92% of TOC) and smouldering (~91% of TOC) combustion (Fig. 2c-d), suggesting abundance of more oxidized POC in these emissions, while smouldering burning of CP consisted

of the smallest WSOC fraction (~46%). These observations point towards the presence of non-polar organic moieties, which are soluble in MeOH but not in water, as previously reported in the literature (Lin et al., 2017).

3.3 Optical properties of Fresh organic aerosol:

597

598

599

600

601

602

603

604

605

606

607

608

609

610

611

612

613

614

615

616

617

618

619

620

621

622

623

Due to the variation in chemical composition and solubility of the fresh BB emissions, we observed substantial diversity in the optical properties of the freshly emitted organic particles. Since MSOC corresponded to >92% of the total OC in our fresh BB emissions, our estimated MSOC concentrations can be used as a proxy for bulk OC. The absorption angstrom exponent (AAE₃₀₀₋₅₅₀, measured in the range of 300-550 nm) of the particles sampled from the fresh emission for different fuels ranged between 4.4-5.3 and 4.7-6.2 for WSOC and MSOC, respectively (Fig. S7). In general, for all samples, AAE_{MSOC} was found to be marginally higher than the respective AAE_{WSOC}. These values fall in the ranges of previously reported AAE for BB emitted as well as urban MSOC and WSOC (Cao et al., 2021; Fan et al., 2018; Yan et al., 2015; Mukherjee et al., 2020). However, our estimated AAE₃₀₀₋₅₅₀ values were higher than reported values from western-US wildfires for similar wavelength range (1.6-1.8, Chakrabarty et al., 2023) and AAE₄₀₁₋₈₇₀ reported from laboratory burns of canopy (2.69±0.36), litter (1.86±0.20) and mixed (2.26±0.36) coniferous ecosystem from western USA (Selimovic et al. 2018). Interestingly, our reported AAE₃₀₀₋₅₅₀ values matched well with lab burning of rotten logs (4.60±3.73) of Douglas fir (Pseudotsuga menziesii) and ponderosa pine (Pinus ponderosa) from Western USA and generally fell in the range of previously reported AAE values from FIREX campaigns (FIREX 2016: McClure et al., 2019; FIREX 2019: Zeng et al., 2022) for emissions with OA/BC ratios ranging from 6.6-143 (McClure et al., 2020) or EC/OC ratios of 0.01-0.3, assuming an average OA/OC ratio of 2. All the flaming dominated and full combustion emissions, as well as some smouldering dominated emissions reported in our work, had EC/OC ratios that fell in this range. The largest variability in AAE_{MSOC} in our study was observed among BFS smouldering (5.5-6.2) and flaming (5.3-6.0) samples, which was likely a result of the difference in combustion and heterogeneous vegetation distribution in the burnt BFS samples. The Svalbard peat (NOR) emission displayed AAE_{WSOC} in the range of 4.6-5.2, while its AAE_{MSOC} was constrained in the range of 4.9-5.2. In comparison to open BB, fresh RWC emissions having high soot contents (Mukherjee et al., 2024; wood stove 1 in Figure S7) exhibited much lower AAE for both WSOC and MSOC (2.2-2.4), while the wood

624 combustions from the previous campaign (Ihalainen et al., 2019a; wood stove 2 in Fig. S7) displayed larger AAE_{WSOC} (5.8-6.8) and AAE_{MSOC} (5-5.6). The lower AAE values of RWC emissions indicates that BrC from 625 626 high EC/OC emissions absorb light throughout the measured spectral range, as shown earlier by Saleh et al. 627 (2018).The MAE values obtained from UV-vis spectroscopy at 365 nm for fresh BB emitted MSOC (MAE_{MSOC} 365) 628 were constrained between 0.46-1.48 m² g⁻¹ for the experiments. In comparison, MAE_{WSOC} 365 was found to 629 630 be in the range of 0.51-1.78 m² g⁻¹. These MAE₃₆₅ values fall within the same range as observed for BBOA in 631 previous literature (Park and Yu, 2016; Huo et al., 2018; Moschos et al., 2018; Cao et al., 2021). In general, flaming dominated BB emissions had higher MAE_{MSOC} 365 values compared to smouldering emissions (Fig. 632 5a). Among open BB experiments, the lowest MAE_{MSOC} 365 were generally observed for fresh emissions from 633 BFS smouldering combustions (0.56±0.10 m² g⁻¹), while flaming combustion of CP (1.31±0.13 m² g⁻¹) and 634 SW (1.06-1.38 m² g⁻¹) were estimated to have the highest MAE_{MSOC} 365 (Table S4). The MAE_{MSOC} 365 for 635 smouldering SG (0.68-0.94 m² g⁻¹) and SW (1.05-1.11 m² g⁻¹) emissions were in a similar range to the 636 MAC_{OA 370} estimated by Vakkari et al. (2025) and agreed well with of MAC₃₇₀ from African residential 637 638 biomass burning emissions (0.24 – 2.2 m² g⁻¹) as reported by Moschos et al. (2024). Previously estimated MAC_{BrC} (at 405 nm) from In-Situ observations made during WE-CAN campaign (2018) in the US and 639 ORACLES-2016 and CLARIFY (2017) campaigns over Southern Africa ranged from 0.9 to 1.6 m² g⁻¹ 640 (Carter et al., 2021). However, it should be noted that our estimated MAE values need to be divided by a 641 642 suitable OA/OC ratio before comparing with MAC_{OA}. In addition, MAE values for high temperature wood 643 log combustion in the modern European stove were significantly higher than for open BB. Fresh RWC emissions had MAE_{MSOC} 365 values in the range of 3.33-16.4 m² g⁻¹, while the MAE_{WSOC} 365 values ranged 644 from 0.32-4.96 m² g⁻¹. The trend between the EC/OC ratios obtained for different experiments to the 645 corresponding MAE_{MSOC} also suggests that EC rich emissions contribute to stronger BrC light absorption 646 647 (Fig. 5a). Formation of BrC internally mixed with soot particles in high temperature BB emissions has been shown to contribute to enhanced light absorption in past studies, due to lensing effect (Jacobson et al., 2001; 648 Liu et al., 2015; Liu et al., 2017; Zhang et al., 2025), which supports our observation. 649

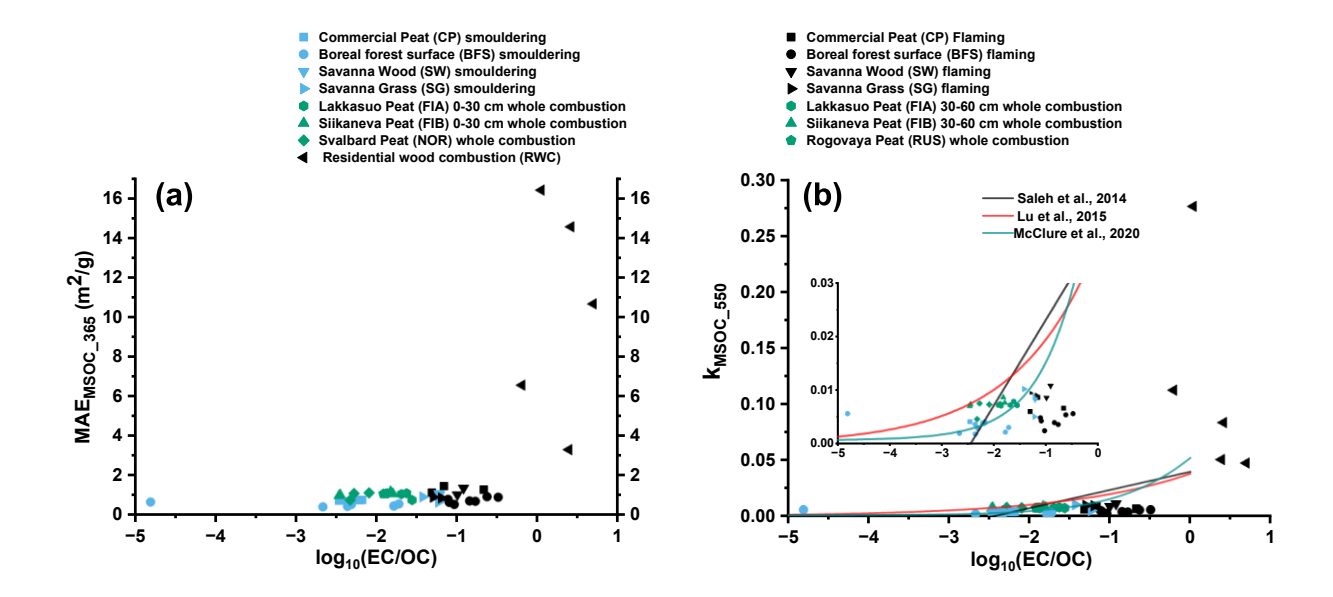


Figure 5: Relationships between MAE_{MSOC_365} (a) and k_{MSOC_550} (b) with EC/OC of open BB and RWC emissions. We observe increasing MAE and k for high temperature combustions with higher EC/OC ratio

The imaginary refractive index measured at the middle of the visible light spectrum at 550 nm (k₅₅₀) for the BB MSOC varied across orders of magnitude and ranged between 0.002-0.011(Fig. 5b, Table S4) in our experiment. Similar to MAE, the smouldering emissions exhibited lower k_{MSOC_550} than the flaming dominated burns. As shown in previous studies (Saleh et al., 2018; Saleh et al., 2020) there seem to exist a continuum between the ratio of EC/OC in the fresh BB emission to the BrC light absorption, as we again observed enhanced k_{MSOC_550} for EC rich wood stove emissions (fig. 5b). Most of the fresh BB MSOC fell in the weak BrC regime in the "k-w" space (Fig. 6a), proposed by Saleh et al. (2018), while some of the wood stove combustion generated particles, in contrast, were in the strong BrC domain. These results fall in line with previous observations of high temperature (and high MCE) biomass combustions generating "darker BrC", which exhibit much stronger light absorption compared to lower temperature open BB emissions (Saleh et al., 2018). The data points in k-w space obtained in this study matches reasonably well with previous literature, as shown in Figure 6a.

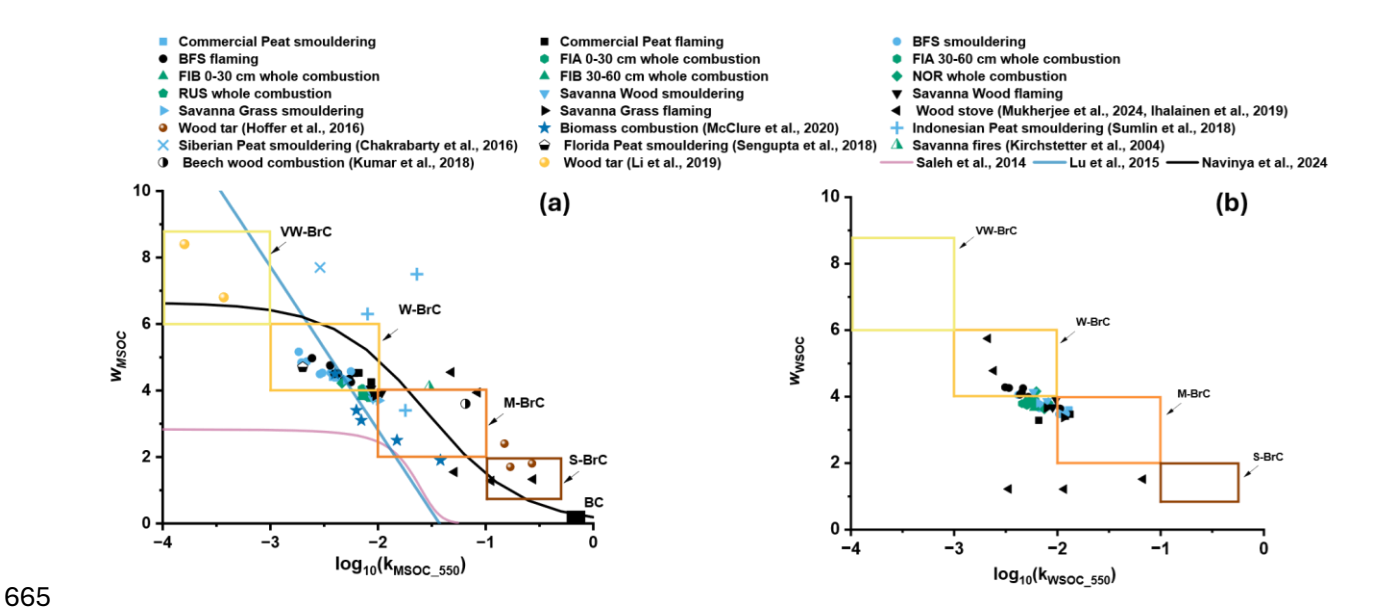


Figure 6: Relationship between w and k₅₅₀ for (a) MSOC and (b) WSOC in fresh emissions from smouldering (light blue points), flaming (black points), full combustion (green points) of open BB performed in this study. Rectangles denote the different light absorbing BrC classes. Several data points from previous literatures (Hoffer et al., 2016; McClure et al., 2020; Sumlin et al., 2018; Chakrabarty et al., 2016; Sengupta et al., 2018; Kirchstetter et al., 2004; Kumar et al., 2018; Li et al., 2019; Saleh et al., 2014; Lu et al., 2015; Navinya et al., 2024) have been added in (a) for reference.

3.4 Particle size distributions and morphologies of chamber diluted primary emissions

Particle size distribution, morphology and effective density were measured for chamber diluted primary emissions. Smouldering combustion of BB generally emitted more particles on average when compared to flaming combustion (Fig. S8). Overall, there was little variability in the particle size distributions for flaming combustion experiments, irrespective of the biomass type. The average particle geometric mean diameters (GMD) ranged between 48 and 85 nm (Table 1). However, we observed clear variation in the emitted particle size distribution among the smouldering combustions, likely due to the unique combustion behaviour of individual samples with varying distributions of different types of biomasses, such as surface vegetation, litter and woody branches. Smouldering combustion of BFS gave rise to distinct bimodal size distributions with the lower mode having a GMD of 30-40 nm, and the larger mode peaking around 100-175 nm. Some replicates of smouldering emissions from CP and SW burning also exhibited bimodal size distribution.

The effective densities of primary particles inside the chamber varied between experimental replicates (Fig S9), which can again be explained by the variability in the combustion and emissions between experiments. The effective densities were largely independent of the particle diameter for all fuel type and combustion conditions (Fig. S9), unlike soot-rich RWC emissions that exhibited size-dependent behaviour in our previous work (Leskinen et al., 2014; Mukherjee et al., 2024). Due to the size-independent behaviour, we averaged over all experimentally obtained density values and estimated average particle densities for each BB emissions (Table S4). While CP and BFS combustion emitted particles had average densities of 1.1 g cm⁻³ and 1.20(±0.05) g cm⁻³ for both smouldering and flaming dominated combustions, SW and SG emitted particles were denser with average densities of 1.4 g cm⁻³ and 1.65(±0.05) g cm⁻³ for smouldering combustion respectively. For flaming combustions, SW emitted primary particles had an average density of 1.45(±0.05) g cm⁻³ and SG particle density was 1.75(±0.05) g cm⁻³. Little to no size-dependency for particle density was observed in our experiments suggesting near-spherical particle morphology with mobility exponents close to 3 (Leskinen et al., 2023; Corbin et al., 2023). SEM images of chamber diluted primary emissions (Fig. S10) support these results, since mostly round organic particles were observed from the collected grids. These findings agree with the measured chemical compositions that indicated that freshly emitted particles consisted mostly of POC and very little EC, leading to formation of particles with a spherical morphology, so-called tarballs. Tarballs have been previously observed in BB emissions (Chakrabarty et al., 2010; China et al., 2013; Hoffer et al., 2016; Adachi et al., 2019) and atmospheric dilution and aging have been shown to aid the formation of spherical viscous tarball BrC (Hennigan et al., 2011; Sedlacek et al., 2018). In chamber diluted CP and BFS emissions, we observed mostly tarballs (Fig. S10a-d) but SG and SW emissions (Fig. S10e-h) also had soot agglomerates that were partially coated or embedded with organics, as previously reported in China et al. (2013). Notably, the morphology of fresh particles emitted from open BB was very different to those emitted from a wood stove (Mukherjee et al., 2024), where the high temperature combustion formed mostly chain-like fractal soot agglomerate structures which were mostly bare or with some organic inclusions (Fig. S10i; China et al., 2013).

709

710

684

685

686

687

688

689

690

691

692

693

694

695

696

697

698

699

700

701

702

703

704

705

706

707

708

3.5 Effect of chamber dilution on the properties of fresh emission aerosols

The relative fractions of OC1, OC2, OC3, OC4, PC and EC in fresh emissions differed before and after dilution in the chamber (Fig.7; Table S3), highlighting the effect of dilution on the overall chemical composition of BB emissions. The relative fraction of the intermediate volatility (IVOC) and semi-volatile organics (SVOC), namely OC1 and OC2 obtained from IMPROVE-A protocol (Ma et al., 2016) were lower in the diluted chamber samples than in the fresh emissions, while the low volatile fractions from OC3 to PC increased (Fig. 7, Table S3). We might have over-estimated the OC1 fraction in fresh emission due to gas phase VOC adsorption on the filter surface causing positive artifact (Kirchstetter et al., 2001). However, the significant increase in low volatile OC fractions (OC3, OC4 and PC) in chamber samples indicate dilution related evaporative loss of the volatile OC fractions in the chamber due to partitioning between gas and particle phase (Calderon-Arrieta et al., 2024).

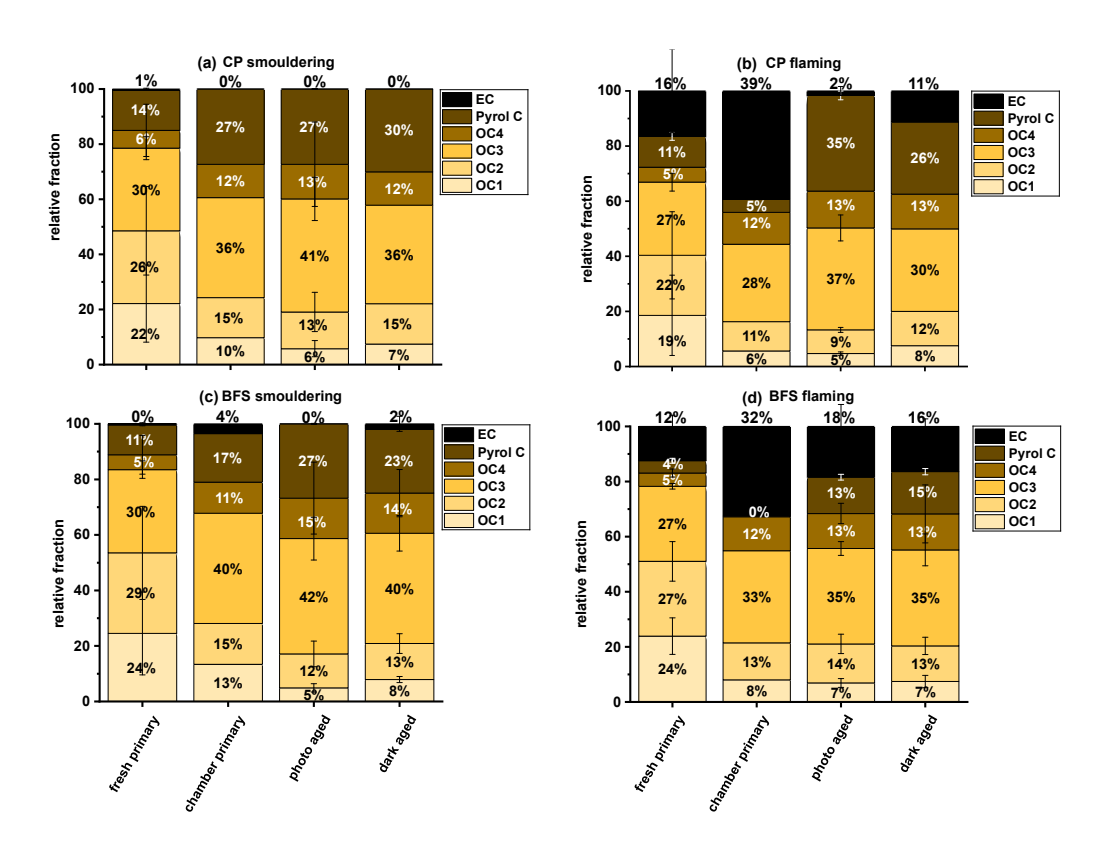


Figure 7: The relative abundance of different OC fractions and EC measured in BB emissions from (a) fresh emission, (b) fresh emission after dilution in chamber, (c) photochemically and (d) dark aged emission in the chamber. Error bar indicates the variability among experimental replicates

The partitioning of OC1 and OC2 fractions between gaseous and condensed phases is largely influenced by the prevailing concentrations in the collected aerosol. Thus, a clear trend is seen between the share of low

volatile OC fractions (OC3+OC4+PC) to the total OC and the collected aerosol OC concentration (Fig. 8). The dilution and consequent evaporation of the most volatile OC also influence the solubility of the POC of the fresh emission. MeOH extraction efficiency significantly decreased for the more diluted POC in the chamber (Fig. S11b). This is in line with the change in volatility as the low volatile OC fraction, including tarball BrC, is generally less soluble in solvents (Chakrabarty et al., 2023; Saleh et al., 2020).

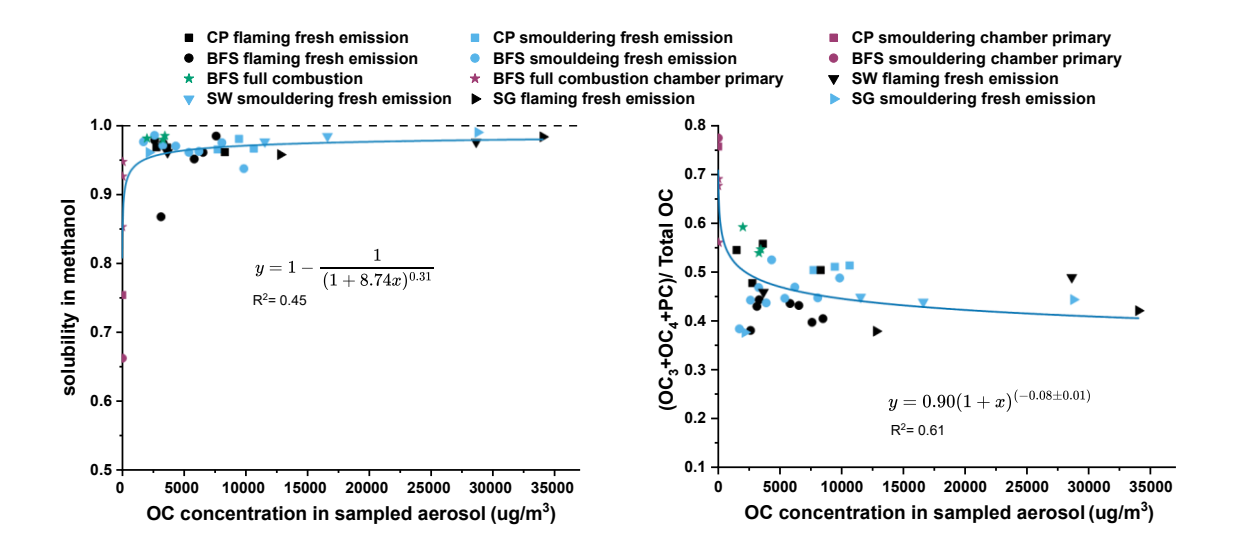


Figure 8: Effect of OC concentration on the partitioning of the OC fractions in BB emissions. Higher dilution in the chamber resulting in lower OC concentration result into larger fraction of low volatile OC fractions and lower solubility in MeOH

The increment in the low volatile OC fractions in chamber diluted primary emissions could also be seen from the abundance of spherical tarballs in the SEM images (Fig. S15). We postulate, based on indirect evidence and previous knowledge, that the fresh BB emission collected on the filters probably had poorly formed tarballs (consisting of higher OC1 and OC2 fractions) and higher MeOH extractable OC. After the dilution related change in volatility distribution of the OC in the chamber (Calderon-Arrieta et al., 2024), MeOH insoluble, highly viscous and spherical tarballs were formed in the chamber (Heninghan et al., 2011; Sedlacek et al., 2018; Adachi and Buseck, 2011). Interestingly, we observed a slight increase in the solubility of WSOC for chamber primary samples (Fig. S11a). This might be the effect of low OC amount filters collecting chamber diluted samples, leading to higher water to OC ratio during the extraction. Thus, the

volume of water used for extracting chamber primary filter punches allowed the dissolution of sparingly water-soluble organics.

The change in particle volatility and solubility due to dilution in the chamber did not significantly affect the light absorption wavelength dependency of MSOC and WSOC. The AAE_{MSOC} and AAE_{WSOC} of chamber diluted samples ranged from 5.5-6.1 and 5-5.9, respectively. At the same time, the AAE_{MSOC} and AAE_{WSOC} for the corresponding freshly emitted particles were 5.3-5.6 and 4.6-5.3, respectively. However, we observed a 17% decrease in MAE_{MSOC_365} (Fig. S12) and a 25% decrease in MAE_{WSOC_365} (Fig. S13) in the chamber primary samples compared to fresh emissions for BFS full combustion samples. This suggests that the fraction of OC extracted by water and MeOH in chamber diluted primary samples had smaller mass absorption efficiency compared to those extracted from the fresh emissions. This can again be explained by the formation of non-soluble dark BrC through the phenomenon termed as "darkening by volatilization" as the low volatile fraction consists of stronger chromophores (Calderon-Arrieta et al., 2024).

3.6. Effects of simulated atmospheric aging on properties of particulate organic matter

3.6.1 Effects of aging on volatility and solubility of OC

The relative OC fractions of chamber diluted primary particles and aged particles seemed to be similar (Fig. 7), suggesting that when it comes to the relative distribution of the OC volatility in BB emissions, the effect of dilution in the environmental chamber outweighed the impact of photo and dark oxidative aging we achieved in our experiments. After oxidative aging there were, however, further increments of the PC, which is the lowest volatility organic fraction. Oxidative aging is known to increase the oxidation state and decrease the volatility of aged particles, making them more insoluble in organic solvents (Saleh et al., 2020).

Expectedly, we observed that both photochemical and dark oxidative aging decreased the fraction of MSOC significantly (Figure S11b). On the other hand, the more oxygenated aged OC exhibited slightly higher WSOC compared to POC in fresh emissions, and we observed a medium correlation (R = 0.5) between water solubility and the atomic O:C ratio obtained from SP-AMS (Fig. S14b). The only exception to this were the smouldering emissions of CP and BFS, which did not exhibit any significant change in water solubility after

dark or photochemical aging. This suggests that the chamber diluted POA emitted from smouldering burns are more resistant to photochemical or dark oxidation, inadvertently hinting towards the highly viscous tarball BrC. Tarballs are known to be resistant to chemical oxidation (Chakrabarty et al., 2023) and we also observed the formation of more stable dark tarballs, especially in smouldering emissions, due to oxidative aging in the chamber (Fig. S15).

3.6.2 Effects of aging on organic matter density

Oxidative aging, both in photochemical and high NO_x dark conditions, led to a marginal increment in particle densities for BFS emissions. For BFS smouldering emission, the effective density after photochemical aging increased to 1.30 ± 0.05 g cm⁻³ while no significant change was observed between primary and dark aged particle densities. For flaming dominated combustion, the particle densities increased under both photochemical (1.30 ± 0.09 g cm⁻³) and dark aging conditions (1.30 ± 0.07 g cm⁻³). For CP, the effective density of high NO_x dark aged particulate emissions remained unaltered at 1.1 g cm⁻³, while photochemically aged emissions exhibited higher density. For SW emissions, both photochemical aging and low NO_x dark aging appeared to have a negligible impact on overall particle effective densities (Table S4). In contrast, particle effective densities for flaming and smouldering combustion of SG emissions seemed to be slightly lower after undergoing photochemical and dark aging (Table S4), although the effects of statistical errors couldn't be discarded due to lack of repetitions of the experiments.

3.6.3 Effects of aging on organic matter chemical composition

Due to low OC loading on the filters collected from the chamber, we were only able to assign roughly 120-600 unique elemental formulae of the most abundant chemical compounds from FT-ICR MS analyses of the photo and dark aged samples of CP and BFS, while signals arising from other compounds were below the detection threshold ($S/N \ge 6$) (Fig. S16, S17). Therefore, we were unable to perform a one-to-one comparison of the chemical compositions of the fresh emission with the chamber-aged samples. However, we could conclude that CH and CHO were the most abundant compound classes in the chamber diluted primary and aged samples for both CP and BFS. We obtained elemental ratios (O:C, H:C and N:C) of the chamber diluted

primary and aged samples from the SP-AMS measurement to characterize the variability in the bulk composition of the OC. The resulting Van-Krevelen plots (Fig. S18) showed that the chamber diluted primary emission had H:C values close to 2.0, while the O:C and N:C values ranged between 0.10-0.25 and 0.013-0.027, respectively. We observed an increment in the O:C ratios in the chamber aged emission while the H:C ratio decreased, as in some previous studies (Lambe et al., 2011). On the other hand, after high NO_x dark aging, the overall N:C ratio did not display a similar increase, probably due to the fast degradation of the nitroaromatics formed inside the chamber at the time of filter collection at the end of the experiments.

3.6.4 Effects of aging on optical properties

799

800

801

802

803

804

805

806

807

808

809

810

811

812

813

814

815

816

817

818

819

820

821

822

823

824

825

Depending on the biomass type and the combustion conditions, photochemical aging either increased (fig. S19b) or decreased (fig. s19a,c,d) the light absorption efficiency (MAE) at wavelengths below 350 nm, while the MAE $_{MSOC}$ at wavelength range 350-450 nm decreased for all cases. Overall, MAE $_{MSOC}$ 550 and k_{MSOC} 550 also decreased and in some cases remain unaltered (Fig. 9, Table S4) after photochemical aging, while w_{MSOC} increased. The w_{WSOC} and w_{MSOC} varied between 3.3-3.7 and 4.3-4.5 respectively for fresh emission of CP, while it increased to 4.0-5.1 and 4.0-6.4 after photochemical aging. The largest increase in w_{MSOC} was observed for flaming combustion of SG, where w_{MSOC} increased from 3.9 to 6.3, while k_{MSOC} 550 decreased an order of magnitude. All the photochemically aged WSOC and MSOC samples in this study lied in the w-BrC to vw-BrC region of the k-w space. This behaviour is in line with the effects of photobleaching and photolysis during OH exposure in the presence of UV lights. Increasing photooxidation has been shown to cause fragmentation reactions after functionalization (Kroll et al., 2015; Saleh et al., 2020). OH has been shown to cleave polyaromatic chains and give rise to short unsaturated chemical moieties that absorb light at the UV range of the spectrum. On the other hand, photochemical aging of RWC emissions in oxidation flow reactor either decreased (for samples from Ihalainen et al., 2019a) or increased (Mukherjee et al., 2024) the k_{MSOC} 550, suggesting that chemical composition of the precursor organic molecules and the reaction pathways are consequential to secondary BrC optical properties (Lambe et al., 2013; Sumlin et al., 2017; Hems et al., 2020). The effect of dark aging on the optical properties was more non-trivial in our study. We noted that for

flaming dominated emissions, the NO_x dominated dark aging led to higher k₅₅₀ values and decreasing w

values (fig. 9) in accordance with Saleh (2020). This suggests an increase in light absorption towards the visible wavelength range, which was also seen in the absorption spectra (fig. S19b,d). On the other hand, dark aging seemed to have minor effect on the smouldering emissions of BFS (Fig.9, Fig. S19a). One explanation for this observation could be the prevalence of tarballs in the smouldering dominated emissions of both peat and other biomass samples, which have been shown to be quite resistant to oxidative aging (Chakrabarty et al., 2023). Additionally, nitroaromatics are reactive, and certain fractions of them may have degraded at the end of the chamber experiments or during filter collection from the chamber, making it difficult to distinguish the effects on optical properties. Owing to very limited NOx concentration in the chamber during the "low-Nox" dark aging, we observed very limited effects of aging on the savanna biomasses. In general, the MAE and k decreased after aging (Table S4), most likely aided by the ozonolysis pathways in the presence of externally injected O3 into the chamber.

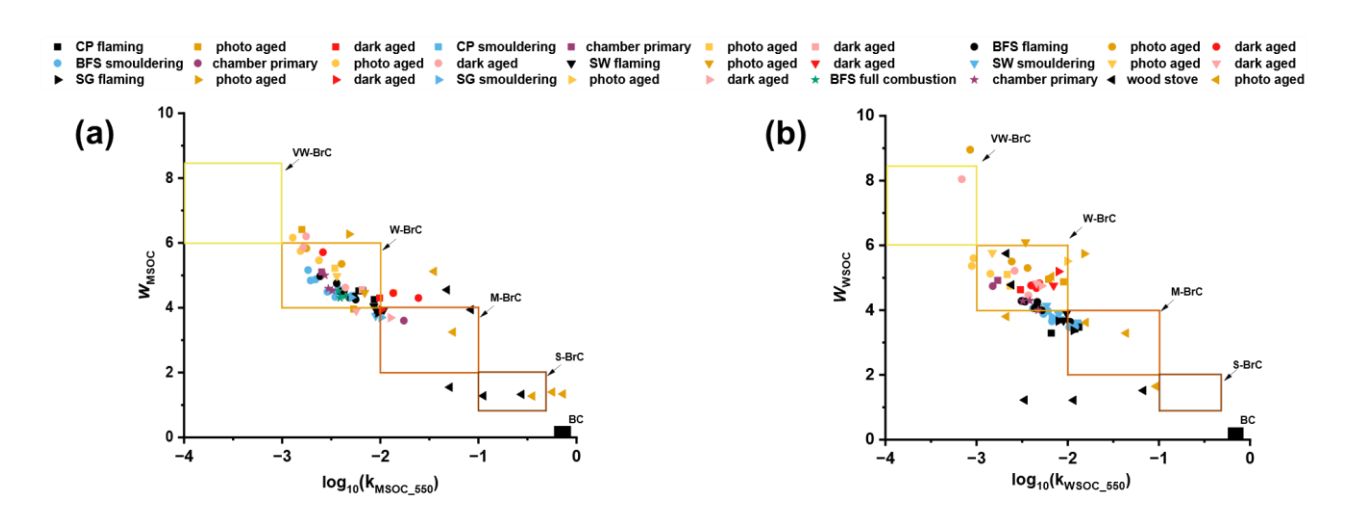


Figure 9: k-w space for all experimental data included in our study. Black, blue and green colours denote fresh emissions from flaming, smouldering and full combustion respectively. Purple dots denote primary emission in chamber without any aging (chamber primary). Dark yellow and red points denote photochemical and dark aging of flaming dominated emissions respectively, while light yellow and red dots represent respective photochemical and dark aging of smouldering dominated emissions.

WSOC light absorption in "k-w space" (fig. 9b) suggests that the water soluble BrC in fresh and aged emissions of RWC had lower k_{550} values and therefore less strongly absorbing chromophores than the corresponding MSOC samples. Certain dark aged samples, especially those for flaming BFS and SG emissions, also seemed to contain stronger chromophores in MSOC than in WSOC (Fig. 9). These observations suggest that less polar organics, which are soluble in MeOH but not in water, contribute to higher light absorption in these BB emissions. In addition, it should be noted that MSOC light absorption in the aged emissions might be underestimated, because fractions of the aged organics were non-soluble (Fig. S12b) and might have contained even stronger chromophores. In future, online measurements of OA absorption at different wavelengths is needed to confirm the observed effects of photochemical and dark aging.

4. Conclusions:

Our estimated OC and EC EFs suggest that OC generally dominates open BB emissions and specifically smouldering conditions emit higher OC than flaming combustion, in agreement with previously existing knowledge. However, we observed significant variation in EFs among experimental replicates, especially for smouldering burns of the same biomasses (fig. 2a,c). This clearly demonstrates how dynamic and variable open BB emissions are inherently, with many factors, including chemical compositions, fuel moisture content and combustion conditions, playing a crucial role in determining the emissions. Emission inventories for open BB from field and lab measurements are often presented as a single value averaged over experimental replicates (Andreae et al., 2019) for air quality or regional climate modelling purposes, and our findings highlight the importance of parameterizing EFs as a function of MCE (Fig. S6) or emitted OA/BC (or OC/EC) ratios for accurate modelling. The estimated high EFoc for boreal and arctic peatland burns in our experiments also indicates that these vegetation types can become a major source for OA emissions in the region in response to increased forest fires, which can have drastic effects on local air quality and climate.

To include the effects of BrC in climate models, an important approach is to parameterize BrC k values as a function of the BC-to-OA (or alternatively EC/OC) ratio of the emissions. The estimated eBC/OA ratios for different fresh BB emissions in our study varied by orders of magnitude and ranged from 0.002 to

0.7. For different climate models, different BC/OA ratios such as 0.03-0.06 (Wang et al. 2018) and 0.08 (Brown et al., 2018) have been used, which don't account for the fuel or combustion phase dependent variations of BC/OA or EC/OC. The k_{MSOC_550} for fresh BB emissions in our study varied between 0.002 and 0.011, and fell into the category of W-BrC, as classified by Saleh (2020). The k values of open BB emissions are very similar to those used in existing models, whereas BrC from high temperature combustion is currently underestimated. We also observed a different trend between k_{MSOC_550} and EC/OC in this work (Fig. 5b) compared to previous literature, suggesting the need for an extensive fuel and combustion dependent emission inventory for better parameterization of BB emitted BrC k values for global climate models.

We observed a strong abundance of tarball morphologies of variable sizes for all open BB emissions, especially for smouldering burns. Characterization of the BB emissions in the environmental chamber revealed that the most volatile OC fractions, OC1 and OC2, decreased in the chamber compared to fresh emissions, due to particle-to-gas partitioning. This dilution-induced change of OC volatility distribution resulted in higher fractions of OC3, OC4 and PC (overlapping with SVOC, LVOC and ELVOC), potentially leading to more absorbing BrC chromophores (Calderon-Arrierta et al., 2024) as well as more defined tar balls in the chamber primary samples. We observed a slight decrease in MAE_{MSOC} for wavelengths higher than 365 nm. This contrasting finding is likely because our solvent extraction method cannot resolve the lowest volatility fraction of organics (with tar ball morphology) in the chamber primary samples.

We determined an increase in O:C ratio of the particles upon photochemical and dark oxidation, which resulted in an increase in ELVOC fractions (PC in particular), making it more insoluble in solvents. Dark aged CP and BFS smouldering emissions in particular had the lowest MeOH solubility, probably due to the observed high abundance of highly viscous, low volatility tarballs (Chakrabarty et al., 2023). For the dark-aged samples, MAE_{MSOC} increased for all wavelengths, suggesting the formation of stronger light-absorbing oxygenated compounds and/or nitroaromatics. For photochemically aged samples, k_{MSOC_550} decreased, probably due to photobleaching and breaking down of BrC chromophores. After aging k_{MSOC_550} values ranged from 0.0011 to 0.03 across all studied biomass types, which were significantly lower than the k₅₅₀ values currently used in climate models. However, our estimated k₅₅₀ values don't include the non-soluble and highly light absorbing s-BrC fractions. Consequently, in future it would be important to

899 combine online and offline optical measurements of open BB emitted OA to characterize also the non-900 soluble organic fraction. Data availability: 901 902 Essential data used in this study are available at FAIR-aligned data repository Zenodo via 903 https://doi.org/10.5281/zenodo.15647186 with Creative Commons Attribution 4.0 International license 904 (Mukherjee et al., 2025). Detailed mass spectrometry data are available upon request from the corresponding 905 authors. 906 907 **Author contribution:** VV, AnV, OS, AH, PYP, MI, KK and AB contributed in designing the study as well as supervising the whole 908 experimental campaign. KK and MR arranged for the arctic-boreal biomasses, whereas KJ, SJS, PGVZ and 909 910 VV collected, sorted and transported savanna biomasses to the study site in Finland. Measurements were performed by AM, MaS, AH, MI, PYP, LMFB, DL, TuK, LV, AB, MuS and VV. Offline filter analyses, 911 including solvent extraction and thermal-optical analyses were performed by AM and VL, with supervisions 912 913 from NK. SEM images were captured by HK. FT- ICR MS analyses of filter samples and subsequent data analyses and plotting were done by CPR, TiK, VHN and JJ. Other data analyses were performed by AM, 914 MaS, TuK, AH, LB and LV. The manuscript was prepared by AM with help from AH, OS, MR, KK, MaS, 915 LB, VN, TK, CR, JJ, HT and AkV. Fundings for this work were acquired by OS, AkV, AnV, VV and HT. 916 917

Acknowledgements:

918

919

920

921

922

The authors would like to thank adj. prof. Minna Väliranta (University of Helsinki), who kindly delivered Arctic and boreal peat samples for this work by within the scope of an Arctic Avenue project. We would also like to acknowledge Dr. Niko Kinnunen (Department of Environmental and Biological Sciences, University of Eastern Finland) for his help regarding the TOC analyses.

Financial support:

923	This work was supported by the Research Council of Finland via the project "Black and Brown Carbon in
924	the Atmosphere and the Cryosphere" (BBrCAC) (decision number 341271), and projects 341597, 355871
925	and 343359 as well as Jane and Aatos Erkko Foundation project "Climate and air quality impacts of boreal
926	forest fires" (BoFF). The authors also gratefully acknowledge Research Council of Finland Flagship
927	fundings (grant no. 337550, 337552) and fundings from the European Commission under the Horizon 2020
928	Research and Innovation Framework Programme, H2020-INFRAIA-2020-1, Grant Agreement
929	number:101008004. A.M acknowledges the LUMETO Doctoral Fellowship provided by the University of
930	Eastern Finland. The mass spectrometry facility is supported by Biocenter Kuopio, Instruct Center Finland

931

933

References:

- 934 Adachi, K., & Buseck, P. R. (2011). Atmospheric tar balls from biomass burning in Mexico. Journal of
- 935 Geophysical Research, 116(D5), D05204. https://doi.org/10.1029/2010JD015102

(FINStruct) and Research Council of Finland (FIRI funding).

- 936 Adachi, K., Sedlacek, A. J., Kleinman, L., Springston, S. R., Wang, J., Chand, D., Hubbe, J. M., Shilling, J.
- 937 E., Onasch, T. B., Kinase, T., Sakata, K., Takahashi, Y., & Buseck, P. R. (2019). Spherical tarball particles
- 938 form through rapid chemical and physical changes of organic matter in biomass-burning smoke.
- 939 Proceedings of the National Academy of Sciences of the United States of America, 116(39), 19336–
- 940 19341. https://doi.org/10.1073/pnas.1900129116
- Adler, G., Wagner, N. L., Lamb, K. D., Manfred, K. M., Schwarz, J. P., Franchin, A., Middlebrook, A. M.,
- 942 Washenfelder, R. A., Womack, C. C., Yokelson, R. J., & Murphy, D. M. (2019). Evidence in biomass
- burning smoke for a light-absorbing aerosol with properties intermediate between brown and black
- 944 carbon. Aerosol Science and Technology, 53(9), 976–989.
- 945 <u>https://doi.org/10.1080/02786826.2019.1617832</u>
- 946 Akagi, S. K., Yokelson, R. J., Wiedinmyer, C., Alvarado, M. J., Reid, J. S., Karl, T., Crounse, J. D., &
- 947 Wennberg, P. O. (2011). Emission factors for open and domestic biomass burning for use in
- 948 atmospheric models. Atmospheric Chemistry and Physics, 11(9), 4039–4072.
- 949 <u>https://doi.org/10.5194/acp-11-4039-2011</u>
- Andreae, M. O. (2019). Emission of trace gases and aerosols from biomass burning An updated
- 951 assessment. Atmospheric Chemistry and Physics, 19(13), 8523–8546. https://doi.org/10.5194/acp-19-
- 952 8523-2019
- 953 Atwi, K., Cheng, Z., El Hajj, O., Perrie, C., & Saleh, R. (2022). A dominant contribution to light
- absorption by methanol-insoluble brown carbon produced in the combustion of biomass fuels
- 955 typically consumed in wildland fires in the United States. Environmental Science: Atmospheres, 2(2),
- 956 182–191. https://doi.org/10.1039/D1EA00065A

- 957 Aurell, J., & Gullett, B. K. (2013). Emission factors from aerial and ground measurements of field and
- 958 laboratory forest burns in the southeastern U.S.: PM2.5, black and brown carbon, VOC, and
- 959 PCDD/PCDF. Environmental Science and Technology, 47(15), 8443–8452.
- 960 <u>https://doi.org/10.1021/es402101k</u>
- 961 Barmet, P., Dommen, J., DeCarlo, P. F., Tritscher, T., Praplan, A. P., Platt, S. M., Prévôt, A. S. H.,
- Donahue, N. M., & Baltensperger, U. (2012). OH clock determination by proton transfer reaction mass
- spectrometry at an environmental chamber. *Atmospheric Measurement Techniques*, 5(3), 647–656.
- 964 <u>https://doi.org/10.5194/amt-5-647-2012</u>
- 965 Bateman, A. P., Walser, M. L., Desyaterik, Y., Laskin, J., Laskin, A., & Nizkorodov, S. A. (2008). The effect
- 966 of solvent on the analysis of secondary organic aerosol using electrospray ionization mass
- 967 spectrometry. Environmental Science and Technology, 42(19), 7341–7346.
- 968 https://doi.org/10.1021/es801226w
- 969 Black, R. R., Aurell, J., Holder, A., George, I. J., Gullett, B. K., Hays, M. D., Geron, C. D., & Tabor, D.
- 970 (2016). Characterization of gas and particle emissions from laboratory burns of peat. Atmospheric
- 971 Environment, 132, 49–57. https://doi.org/10.1016/j.atmosenv.2016.02.024
- 972 Bluvshtein, N., Lin, P., Michel Flores, J., Segev, L., Mazar, Y., Tas, E., Snider, G., Weagle, C., Brown, S. S.,
- 973 Laskin, A., & Rudich, Y. (2017). Broadband optical properties of biomass-burning aerosol and
- 974 identification of brown carbon chromophores. Journal of Geophysical Research, 122(10), 5441–5456.
- 975 <u>https://doi.org/10.1002/2016JD026230</u>
- 976 Bond, T. C., & Bergstrom, R. W. (2006). Light absorption by carbonaceous particles: An investigative
- 977 review. In Aerosol Science and Technology (Vol. 40, Issue 1, pp. 27–67).
- 978 https://doi.org/10.1080/02786820500421521
- 979 Bond, T. C., Doherty, S. J., Fahey, D. W., Forster, P. M., Berntsen, T., DeAngelo, B. J., Flanner, M. G.,
- 980 Ghan, S., Kärcher, B., Koch, D., Kinne, S., Kondo, Y., Quinn, P. K., Sarofim, M. C., Schultz, M. G., Schulz,
- 981 M., Venkataraman, C., Zhang, H., Zhang, S., ... Zender, C. S. (2013). Bounding the role of black carbon
- 982 in the climate system: A scientific assessment. Journal of Geophysical Research: Atmospheres,
- 983 *118*(11), 5380–5552. <u>https://doi.org/10.1002/jgrd.50171</u>
- Bond, T., Venkataraman, C., & Masera, O. (2004). Global atmospheric impacts of residential fuels.
- 985 Energy for Sustainable Development, 8(3), 20–32. https://doi.org/10.1016/S0973-0826(08)60464-0
- 986 Bosch, C., Andersson, A., Kirillova, E. N., Budhavant, K., Tiwari, S., Praveen, P. S., Russell, L. M., Beres,
- 987 N. D., Ramanathan, V., & Gustafsson, Ö. (2014). Source-diagnostic dual-isotope composition and
- optical properties of water-soluble organic carbon and elemental carbon in the South Asian outflow
- 989 intercepted over the Indian Ocean. Journal of Geophysical Research: Atmospheres, 119(20), 11,743-
- 990 11,759. https://doi.org/10.1002/2014JD022127
- 991 Brown, H., Liu, X., Feng, Y., Jiang, Y., Wu, M., Lu, Z., Wu, C., Murphy, S., & Pokhrel, R. (2018). Radiative
- 992 effect and climate impacts of brown carbon with the Community Atmosphere Model (CAM5).
- 993 Atmospheric Chemistry and Physics, 18(24), 17745–17768. https://doi.org/10.5194/acp-18-17745-
- 994 2018
- 995 Budisulistiorini, S. H., Riva, M., Williams, M., Chen, J., Itoh, M., Surratt, J. D., & Kuwata, M. (2017).
- 996 Light-Absorbing Brown Carbon Aerosol Constituents from Combustion of Indonesian Peat and
- 997 Biomass. Environmental Science and Technology, 51(8), 4415–4423.
- 998 <u>https://doi.org/10.1021/acs.est.7b00397</u>

- 999 Calderon-Arrieta, D., Morales, A. C., Hettiyadura, A. P. S., Estock, T. M., Li, C., Rudich, Y., & Laskin, A.
- 1000 (2024). Enhanced Light Absorption and Elevated Viscosity of Atmospheric Brown Carbon through
- 1001 Evaporation of Volatile Components. Environmental Science and Technology, 58(17), 7493–7504.
- 1002 <u>https://doi.org/10.1021/acs.est.3c10184</u>
- 1003 Cao, T., Li, M., Zou, C., Fan, X., Song, J., Jia, W., Yu, C., Yu, Z., & Peng, P. (2021). Chemical composition,
- optical properties, and oxidative potential of water- and methanol-soluble organic compounds
- 1005 emitted from the combustion of biomass materials and coal. Atmospheric Chemistry and Physics,
- 1006 *21*(17), 13187–13205. https://doi.org/10.5194/acp-21-13187-2021
- 1007 Carter, T. S., Heald, C. L., Cappa, C. D., Kroll, J. H., Campos, T. L., Coe, H., Cotterell, M. I., Davies, N.
- 1008 W., Farmer, D. K., Fox, C., Garofalo, L. A., Hu, L., Langridge, J. M., Levin, E. J. T., Murphy, S. M., Pokhrel,
- 1009 R. P., Shen, Y., Szpek, K., Taylor, J. W., & Wu, H. (2021). Investigating Carbonaceous Aerosol and Its
- 1010 Absorption Properties From Fires in the Western United States (WE-CAN) and Southern Africa
- 1011 (ORACLES and CLARIFY). Journal of Geophysical Research: Atmospheres, 126(15).
- 1012 <u>https://doi.org/10.1029/2021JD034984</u>
- 1013 Chakrabarty, R. K., Gyawali, M., Yatavelli, R. L. N., Pandey, A., Watts, A. C., Knue, J., Chen, L. W. A.,
- 1014 Pattison, R. R., Tsibart, A., Samburova, V., & Moosmüller, H. (2016). Brown carbon aerosols from
- burning of boreal peatlands: Microphysical properties, emission factors, and implications for direct
- radiative forcing. Atmospheric Chemistry and Physics, 16(5), 3033–3040. https://doi.org/10.5194/acp-
- 1017 16-3033-2016
- 1018 Chakrabarty, R. K., Moosmüller, H., Chen, L. W. A., Lewis, K., Arnott, W. P., Mazzoleni, C., Dubey, M. K.,
- 1019 Wold, C. E., Hao, W. M., & Kreidenweis, S. M. (2010). Brown carbon in tar balls from smoldering
- biomass combustion. *Atmospheric Chemistry and Physics*, 10(13), 6363–6370.
- 1021 https://doi.org/10.5194/acp-10-6363-2010
- 1022 Chakrabarty, R. K., Shetty, N. J., Thind, A. S., Beeler, P., Sumlin, B. J., Zhang, C., Liu, P., Idrobo, J. C.,
- Adachi, K., Wagner, N. L., Schwarz, J. P., Ahern, A., Sedlacek, A. J., Lambe, A., Daube, C., Lyu, M., Liu,
- 1024 C., Herndon, S., Onasch, T. B., & Mishra, R. (2023). Shortwave absorption by wildfire smoke dominated
- by dark brown carbon. *Nature Geoscience*, *16*(8), 683–688. https://doi.org/10.1038/s41561-023-
- 1026 <u>01237-9</u>
- 1027 Chen, K., Raeofy, N., Lum, M., Mayorga, R., Woods, M., Bahreini, R., Zhang, H., & Lin, Y. H. (2022).
- 1028 Solvent effects on chemical composition and optical properties of extracted secondary brown carbon
- 1029 constituents. Aerosol Science and Technology, 56(10), 917–930.
- 1030 https://doi.org/10.1080/02786826.2022.2100734
- 1031 Chen, Y., & Bond, T. C. (2010). Light absorption by organic carbon from wood combustion.
- 1032 Atmospheric Chemistry and Physics, 10(4), 1773–1787. https://doi.org/10.5194/acp-10-1773-2010
- 1033 Cheng, Y., He, K., Engling, G., Weber, R., Liu, J., Du, Z., & Dong, S. (2017). Brown and black carbon in
- 1034 Beijing aerosol: Implications for the effects of brown coating on light absorption by black carbon.
- 1035 Science of The Total Environment, 599–600, 1047–1055.
- 1036 <u>https://doi.org/10.1016/j.scitotenv.2017.05.061</u>
- 1037 China, S., Mazzoleni, C., Gorkowski, K., Aiken, A. C., & Dubey, M. K. (2013). Morphology and mixing
- state of individual freshly emitted wildfire carbonaceous particles. Nature Communications, 4.
- 1039 <u>https://doi.org/10.1038/ncomms3122</u>

- 1040 Chow, J. C., Watson, J. G., Chen, L.-W. A., Chang, M. C. O., Robinson, N. F., Trimble, D., & Kohl, S.
- 1041 (2007). The IMPROVE_A Temperature Protocol for Thermal/Optical Carbon Analysis: Maintaining
- 1042 Consistency with a Long-Term Database. Journal of the Air & Waste Management Association, 57(9),
- 1043 1014–1023. https://doi.org/10.3155/1047-3289.57.9.1014
- 1044 Christian, T. J., Kleiss, B., Yokelson, R. J., Holzinger, R., Crutzen, P. J., Hao, W. M., Saharjo, B. H., &
- 1045 Ward, D. E. (2003). Comprehensive laboratory measurements of biomass-burning emissions: 1.
- 1046 Emissions from Indonesian, African, and other fuels. Journal of Geophysical Research: Atmospheres,
- 1047 108(D23), 4719. https://doi.org/10.1029/2003jd003704
- 1048 Corbin, J. C., Modini, R. L., & Gysel-Beer, M. (2023). Mechanisms of soot-aggregate restructuring and
- 1049 compaction. Aerosol Science and Technology, 57(2), 89–111.
- 1050 https://doi.org/10.1080/02786826.2022.2137385
- 1051 Costa, H., De Rigo, D., Libertà, G., Houston Durrant, T., & San-Miguel-Ayanz, J. (2020). European
- 1052 wildfire danger and vulnerability in a changing climate Towards integrating risk dimensions JRC
- 1053 PESETA IV project Task 9 forest fires. Publications Office of the European Union.
- 1054 <u>https://doi.org/10.2760/46951</u>
- De Rigo, D., Libertà, G., Houston Durrant, T., Artés Vivancos, T., & San-Miguel-Ayanz, J. (2017). Forest
- 1056 fire danger extremes in Europe under climate change Variability and uncertainty. Publications Office
- 1057 of the European Union. https://doi.org/10.2760/13180
- 1058 De Groot, W. J., Flannigan, M. D., & Cantin, A. S. (2013). Climate change impacts on future boreal fire
- 1059 regimes. Forest Ecology and Management, 294, 35–44. https://doi.org/10.1016/j.foreco.2012.09.027
- Desgroux, P., Mercier, X., & Thomson, K. A. (2013). Study of the formation of soot and its precursors in
- 1061 flames using optical diagnostics. *Proceedings of the Combustion Institute*, *34*(1), 1713–1738.
- 1062 <u>https://doi.org/10.1016/j.proci.2012.09.004</u>
- 1063 Desservettaz, M., Paton-Walsh, C., Griffith, D. W. T., Kettlewell, G., Keywood, M. D., Vanderschoot, M.
- 1064 V., Ward, J., Mallet, M. D., Milic, A., Miljevic, B., Ristovski, Z. D., Howard, D., Edwards, G. C., & Atkinson,
- 1065 B. (2017). Emission factors of trace gases and particles from tropical savanna fires in Australia. *Journal*
- of Geophysical Research: Atmospheres, 122(11), 6059–6074. https://doi.org/10.1002/2016JD025925
- 1067 Engling, G., Carrico, C. M., Kreidenweis, S. M., Collett Jr., J. L., Day, D. E., Malm, W. C., Lincoln, E., Min
- Hao, W., Iinuma, Y., & Herrmann, H. (2006). Determination of levoglucosan in biomass combustion
- aerosol by high-performance anion-exchange chromatography with pulsed amperometric detection.
- 1070 Atmospheric Environment, 40, 299–311. https://doi.org/10.1016/j.atmosenv.2005.12.069
- 1071 Faccinetto, A., Desgroux, P., Ziskind, M., Therssen, E., & Focsa, C. (2011). High-sensitivity detection of
- 1072 polycyclic aromatic hydrocarbons adsorbed onto soot particles using laser desorption/laser
- 1073 ionization/time-of-flight mass spectrometry: An approach to studying the soot inception process in
- 1074 low-pressure flames. Combustion and Flame, 158(2), 227–239.
- 1075 <u>https://doi.org/10.1016/j.combustflame.2010.08.012</u>
- 1076 Fan, X., Li, M., Cao, T., Cheng, C., Li, F., Xie, Y., Wei, S., Song, J., & Peng, P. (2018). Optical properties
- and oxidative potential of water- and alkaline-soluble brown carbon in smoke particles emitted from
- 1078 laboratory simulated biomass burning. *Atmospheric Environment*, 194, 48–57.
- 1079 <u>https://doi.org/10.1016/j.atmosenv.2018.09.025</u>

- 1080 Feyen, L., Ciscar, J., Gosling, S., Ibarreta, D., & Soria, A. (2020). Climate change impacts and
- 1081 adaptation in Europe JRC PESETA IV final report (D. Ibarreta & A. Soria, Eds.). Publications Office.
- 1082 <u>https://doi.org/10.2760/171121</u>
- 1083 Fleming, L. T., Lin, P., Roberts, J. M., Selimovic, V., Yokelson, R., Laskin, J., Laskin, A., & Nizkorodov, S.
- 1084 A. (2020). Molecular composition and photochemical lifetimes of brown carbon chromophores in
- biomass burning organic aerosol. *Atmospheric Chemistry and Physics*, 20(2), 1105–1129.
- 1086 <u>https://doi.org/10.5194/acp-20-1105-2020</u>
- Hallar, A. G., Lowenthal, D. H., Clegg, S. L., Samburova, V., Taylor, N., Mazzoleni, L. R., Zielinska, B. K.,
- 1088 Kristensen, T. B., Chirokova, G., McCubbin, I. B., Dodson, C., & Collins, D. (2013). Chemical and
- 1089 hygroscopic properties of aerosol organics at Storm Peak Laboratory. Journal of Geophysical
- 1090 Research: Atmospheres, 118(10), 4767–4779. https://doi.org/10.1002/jgrd.50373
- Hartikainen, A., Tiitta, P., Ihalainen, M., Yli-Pirilä, P., Orasche, J., Czech, H., Kortelainen, M., Lamberg,
- H., Suhonen, H., Koponen, H., Hao, L., Zimmermann, R., Jokiniemi, J., Tissari, J., & Sippula, O. (2020).
- 1093 Photochemical transformation of residential wood combustion emissions: Dependence of organic
- aerosol composition on OH exposure. Atmospheric Chemistry and Physics, 20(11), 6357–6378.
- 1095 https://doi.org/10.5194/acp-20-6357-2020
- Hecobian, A., Zhang, X., Zheng, M., Frank, N., Edgerton, E. S., & Weber, R. J. (2010). Water-Soluble
- 1097 Organic Aerosol material and the light-absorption characteristics of aqueous extracts measured over
- the Southeastern United States. *Atmospheric Chemistry and Physics*, 10(13), 5965–5977.
- 1099 <u>https://doi.org/10.5194/acp-10-5965-2010</u>
- Hems, R. F., Schnitzler, E. G., Bastawrous, M., Soong, R., Simpson, A. J., & Abbatt, J. P. D. (2020).
- 1101 Aqueous Photoreactions of Wood Smoke Brown Carbon. ACS Earth and Space Chemistry, 4(7), 1149-
- 1102 1160. https://doi.org/10.1021/acsearthspacechem.0c00117
- Hems, R. F., Schnitzler, E. G., Liu-Kang, C., Cappa, C. D., & Abbatt, J. P. D. (2021). Aging of Atmospheric
- 1104 Brown Carbon Aerosol. ACS Earth and Space Chemistry, 5(4), 722–748.
- 1105 https://doi.org/10.1021/acsearthspacechem.0c00346
- 1106 Hennigan, C. J., Miracolo, M. A., Engelhart, G. J., May, A. A., Presto, A. A., Lee, T., Sullivan, A. P.,
- 1107 McMeeking, G. R., Coe, H., Wold, C. E., Hao, W. M., Gilman, J. B., Kuster, W. C., De Gouw, J., Schichtel,
- 1108 B. A., Collett, J. L., Kreidenweis, S. M., & Robinson, A. L. (2011). Chemical and physical
- transformations of organic aerosol from the photo-oxidation of open biomass burning emissions in an
- 1110 environmental chamber. Atmospheric Chemistry and Physics, 11(15), 7669–7686.
- 1111 https://doi.org/10.5194/acp-11-7669-2011
- 1112 Hoffer, A., Tóth, A., Nyir A'-Kósa, I., Pósfai, M., & Gelencsér, A. (2016). Light absorption properties of
- 1113 laboratory-generated tar ball particles. Atmospheric Chemistry and Physics, 16(1), 239–246.
- 1114 <u>https://doi.org/10.5194/acp-16-239-2016</u>
- 1115 Hoffer, A., Tóth, Á., Pósfai, M., Chung, C. E., & Gelencsér, A. (2017). Brown carbon absorption in the red
- and near-infrared spectral region. *Atmospheric Measurement Techniques*, 10(6), 2353–2359.
- 1117 https://doi.org/10.5194/amt-10-2353-2017
- 1118 Huang, R. J., Yang, L., Cao, J., Chen, Y., Chen, Q., Li, Y., Duan, J., Zhu, C., Dai, W., Wang, K., Lin, C., Ni,
- 1119 H., Corbin, J. C., Wu, Y., Zhang, R., Tie, X., Hoffmann, T., O'Dowd, C., & Dusek, U. (2018). Brown
- 1120 Carbon Aerosol in Urban Xi'an, Northwest China: The Composition and Light Absorption Properties.
- 1121 Environmental Science and Technology, 52(12), 6825–6833. https://doi.org/10.1021/acs.est.8b02386

- Huo, Y., Li, M., Jiang, M., & Qi, W. (2018). Light absorption properties of HULIS in primary particulate
- 1123 matter produced by crop straw combustion under different moisture contents and stacking modes.
- 1124 Atmospheric Environment, 191, 490–499. https://doi.org/10.1016/j.atmosenv.2018.08.038
- 1125 Ihalainen, M., Jalava, P., Ihantola, T., Kasurinen, S., Uski, O., Sippula, O., Hartikainen, A., Tissari, J.,
- 1126 Kuuspalo, K., Lähde, A., Hirvonen, M.-R., & Jokiniemi, J. (2019a). Design and validation of an air-liquid
- interface (ALI) exposure device based on thermophoresis. Aerosol Science and Technology, 53(2),
- 1128 133–145. https://doi.org/10.1080/02786826.2018.1556775
- 1129 Ihalainen, M., Tiitta, P., Czech, H., Yli-Pirilä, P., Hartikainen, A., Kortelainen, M., Tissari, J., Stengel, B.,
- 1130 Sklorz, M., Suhonen, H., Lamberg, H., Leskinen, A., Kiendler-Scharr, A., Harndorf, H., Zimmermann, R.,
- 1131 Jokiniemi, J., & Sippula, O. (2019b). A novel high-volume Photochemical Emission Aging flow tube
- 1132 Reactor (PEAR). Aerosol Science and Technology, 53(3), 276–294.
- 1133 <u>https://doi.org/10.1080/02786826.2018.1559918</u>
- 1134 Iinuma, Y., Brüggemann, E., Gnauk, T., Müller, K., Andreae, M. O., Helas, G., Parmar, R., & Herrmann,
- 1135 H. (2007a). Source characterization of biomass burning particles: The combustion of selected
- 1136 European conifers, African hardwood, savanna grass, and German and Indonesian peat. Journal of
- 1137 Geophysical Research: Atmospheres, 112(D8), D08209. https://doi.org/10.1029/2006JD007120
- 1138 Jacobson, M. Z. (2000). A physically-based treatment of elemental carbon optics: Implications for
- 1139 global direct forcing of aerosols. Geophysical Research Letters, 27(2), 217–220.
- 1140 <u>https://doi.org/10.1029/1999GL010968</u>
- 1141 Jacobson, M. Z. (2001). Strong radiative heating due to the mixing state of black carbon in atmospheric
- 1142 aerosols. *Nature*, 409(6821), 695–697. https://doi.org/10.1038/35055518
- 1143 Jayarathne, T., Stockwell, C. E., Gilbert, A. A., Daugherty, K., Cochrane, M. A., Ryan, K. C., Putra, E. I.,
- 1144 Saharjo, B. H., Nurhayati, A. D., Albar, I., Yokelson, R. J., & Stone, E. A. (2018). Chemical
- characterization of fine particulate matter emitted by peat fires in Central Kalimantan, Indonesia,
- 1146 during the 2015 El Niño. Atmospheric Chemistry and Physics, 18(4), 2585–2600.
- 1147 https://doi.org/10.5194/acp-18-2585-2018
- Jennings, S. G., Pinnick, R. G., & Gillespie, J. B. (1979). Relation between absorption coefficient and
- imaginary index of atmospheric aerosol constituents. *Applied Optics*, 18(9), 1368.
- 1150 <u>https://doi.org/10.1364/AO.18.001368</u>
- 1151 Kirchstetter, T. W., Corrigan, C. E., & Novakov, T. (2001). Laboratory and field investigation of the
- 1152 adsorption of gaseous organic compounds onto quartz filters. Atmospheric Environment, 35(9), 1663–
- 1153 1671. https://doi.org/10.1016/S1352-2310(00)00448-9
- 1154 Kirchstetter, T. W., Novakov, T., & Hobbs, P. V. (2004). Evidence that the spectral dependence of light
- absorption by aerosols is affected by organic carbon. Journal of Geophysical Research: Atmospheres,
- 1156 109(D21), D21208. https://doi.org/10.1029/2004JD004999
- 1157 Kirillova, E. N., Andersson, A., Han, J., Lee, M., & Gustafsson, Ö. (2014). Sources and light absorption
- of water-soluble organic carbon aerosols in the outflow from northern China. Atmospheric Chemistry
- and Physics, 14(3), 1413–1422. https://doi.org/10.5194/acp-14-1413-2014
- 1160 Koch, B. P., & Dittmar, T. (2006). From mass to structure: an aromaticity index for high-resolution mass
- data of natural organic matter. Rapid Communications in Mass Spectrometry, 20(5), 926–932.
- 1162 <u>https://doi.org/10.1002/rcm.2386</u>

- 1163 Kodros, J. K., Kaltsonoudis, C., Paglione, M., Florou, K., Jorga, S., Vasilakopoulou, C., Cirtog, M.,
- 1164 Cazaunau, M., Picquet-Varrault, B., Nenes, A., & Pandis, S. N. (2022). Secondary aerosol formation
- 1165 during the dark oxidation of residential biomass burning emissions. *Environmental Science*:
- 1166 Atmospheres, 2(5), 1221–1236. https://doi.org/10.1039/D2EA00031H
- Kodros, J. K., Papanastasiou, D. K., Paglione, M., Masiol, M., Squizzato, S., Florou, K., Skyllakou, K.,
- 1168 Kaltsonoudis, C., Nenes, A., & Pandis, S. N. (2020). Rapid dark aging of biomass burning as an
- overlooked source of oxidized organic aerosol. *Proceedings of the National Academy of Sciences*,
- 1170 *117*(52), 33028–33033. <u>https://doi.org/10.1073/pnas.2010365117</u>
- 1171 Kourtchev, I., Hellebust, S., Bell, J. M., O'Connor, I. P., Healy, R. M., Allanic, A., Healy, D., Wenger, J. C.,
- 1172 & Sodeau, J. R. (2011). The use of polar organic compounds to estimate the contribution of domestic
- 1173 solid fuel combustion and biogenic sources to ambient levels of organic carbon and PM2.5 in Cork
- 1174 Harbour, Ireland. Science of The Total Environment, 409(11), 2143–2155.
- 1175 <u>https://doi.org/10.1016/j.scitotenv.2011.02.027</u>
- 1176 Krawchuk, M. A., Cumming, S. G., & Flannigan, M. D. (2009). Predicted changes in fire weather suggest
- 1177 increases in lightning fire initiation and future area burned in the mixedwood boreal forest. Climatic
- 1178 Change, 92(1–2), 83–97. https://doi.org/10.1007/s10584-008-9460-7
- 1179 Kroll, J. H., Donahue, N. M., Jimenez, J. L., Kessler, S. H., Canagaratna, M. R., Wilson, K. R., Altieri, K. E.,
- 1180 Mazzoleni, L. R., Wozniak, A. S., Bluhm, H., Mysak, E. R., Smith, J. D., Kolb, C. E., & Worsnop, D. R.
- 1181 (2011). Carbon oxidation state as a metric for describing the chemistry of atmospheric organic
- 1182 aerosol. *Nature Chemistry*, 3(2), 133–139. https://doi.org/10.1038/nchem.948
- 1183 Kroll, J. H., Lim, C. Y., Kessler, S. H., & Wilson, K. R. (2015). Heterogeneous Oxidation of Atmospheric
- 1184 Organic Aerosol: Kinetics of Changes to the Amount and Oxidation State of Particle-Phase Organic
- 1185 Carbon. The Journal of Physical Chemistry A, 119(44), 10767–10783.
- 1186 <u>https://doi.org/10.1021/acs.jpca.5b06946</u>
- 1187 Kumar, N. K., Corbin, J. C., Bruns, E. A., Massabó, D., Slowik, J. G., Drinovec, L., Močnik, G., Prati, P.,
- 1188 Vlachou, A., Baltensperger, U., Gysel, M., El-Haddad, I., & Prévôt, A. S. H. (2018). Production of
- particulate brown carbon during atmospheric aging of residential wood-burning emissions.
- 1190 Atmospheric Chemistry and Physics, 18(24), 17843–17861. https://doi.org/10.5194/acp-18-17843-
- 1191 2018
- Lambe, A. T., Ahern, A. T., Williams, L. R., Slowik, J. G., Wong, J. P. S., Abbatt, J. P. D., Brune, W. H., Ng,
- 1193 N. L., Wright, J. P., Croasdale, D. R., Worsnop, D. R., Davidovits, P., & Onasch, T. B. (2011).
- 1194 Characterization of aerosol photooxidation flow reactors: heterogeneous oxidation, secondary organic
- 1195 aerosol formation and cloud condensation nuclei activity measurements. Atmospheric Measurement
- 1196 Techniques, 4(3), 445–461. https://doi.org/10.5194/amt-4-445-2011
- 1197 Lambe, A. T., Cappa, C. D., Massoli, P., Onasch, T. B., Forestieri, S. D., Martin, A. T., Cummings, M. J.,
- 1198 Croasdale, D. R., Brune, W. H., Worsnop, D. R., & Davidovits, P. (2013). Relationship between oxidation
- 1199 level and optical properties of secondary organic aerosol. Environmental Science and Technology,
- 1200 47(12), 6349–6357. https://doi.org/10.1021/es401043j
- 1201 Laskin, A., Laskin, J., & Nizkorodov, S. A. (2015). Chemistry of Atmospheric Brown Carbon. Chemical
- 1202 Reviews, 115(10), 4335–4382. https://doi.org/10.1021/cr5006167
- 1203 Leskinen, A., Yli-Pirilä, P., Kuuspalo, K., Sippula, O., Jalava, P., Hirvonen, M.-R., Jokiniemi, J., Virtanen,
- 1204 A., Komppula, M., & Lehtinen, K. E. J. (2015). Characterization and testing of a new environmental

- 1205 chamber. Atmospheric Measurement Techniques, 8(6), 2267–2278. https://doi.org/10.5194/amt-8-
- 1206 2267-2015
- 1207 Leskinen, J., Hartikainen, A., Väätäinen, S., Ihalainen, M., Virkkula, A., Mesceriakovas, A., Tiitta, P.,
- 1208 Miettinen, M., Lamberg, H., Czech, H., Yli-Pirilä, P., Tissari, J., Jakobi, G., Zimmermann, R., & Sippula,
- 1209 O. (2023). Photochemical Aging Induces Changes in the Effective Densities, Morphologies, and
- 1210 Optical Properties of Combustion Aerosol Particles. Environmental Science and Technology, 57(13),
- 1211 5137–5148. https://doi.org/10.1021/acs.est.2c04151
- Leskinen, J., Ihalainen, M., Torvela, T., Kortelainen, M., Lamberg, H., Tiitta, P., Jakobi, G., Grigonyte, J.,
- 1213 Joutsensaari, J., Sippula, O., Tissari, J., Virtanen, A., Zimmermann, R., & Jokiniemi, J. (2014). Effective
- density and morphology of particles emitted from small-scale combustion of various wood fuels.
- 1215 Environmental Science and Technology, 48(22), 13298–13306. https://doi.org/10.1021/es502214a
- 1216 Li, C., Chen, P., Kang, S., Yan, F., Hu, Z., Qu, B., & Sillanpää, M. (2016). Concentrations and light
- 1217 absorption characteristics of carbonaceous aerosol in PM 2.5 and PM 10 of Lhasa city, the Tibetan
- 1218 Plateau. Atmospheric Environment, 127, 340–346. https://doi.org/10.1016/j.atmosenv.2015.12.059
- 1219 Li, C., He, Q., Hettiyadura, A. P. S., Käfer, U., Shmul, G., Meidan, D., Zimmermann, R., Brown, S. S.,
- 1220 George, C., Laskin, A., & Rudich, Y. (2019). Formation of secondary brown carbon in biomass burning
- aerosol proxies through no3 radical reactions. Environmental Science and Technology, 54(3), 1395–
- 1222 1405. https://doi.org/10.1021/acs.est.9b05641
- 1223 Li, X., Xiao, M., Xu, X., Zhou, J., Yang, K., Wang, Z., Zhang, W., Hopke, P. K., Hopke, P. K., Zhao, W., & Li,
- 1224 X. (2020). Light Absorption Properties of Organic Aerosol from Wood Pyrolysis: Measurement Method
- 1225 Comparison and Radiative Implications. *Environmental Science and Technology*, 54(12), 7156–7164.
- 1226 https://doi.org/10.1021/acs.est.0c01475
- 1227 Li, Y., Pöschl, U., & Shiraiwa, M. (2016). Molecular corridors and parameterizations of volatility in the
- 1228 chemical evolution of organic aerosols. Atmospheric Chemistry and Physics, 16(5), 3327–3344.
- 1229 <u>https://doi.org/10.5194/acp-16-3327-2016</u>
- 1230 Lin, P., Bluvshtein, N., Rudich, Y., Nizkorodov, S. A., Laskin, J., & Laskin, A. (2017). Molecular Chemistry
- 1231 of Atmospheric Brown Carbon Inferred from a Nationwide Biomass Burning Event. Environmental
- 1232 Science and Technology, 51(20), 11561–11570. https://doi.org/10.1021/acs.est.7b02276
- Lin, P., Rincon, A. G., Kalberer, M., & Yu, J. Z. (2012). Elemental Composition of HULIS in the Pearl River
- 1234 Delta Region, China: Results Inferred from Positive and Negative Electrospray High Resolution Mass
- 1235 Spectrometric Data. Environmental Science & Technology, 46(14), 7454–7462.
- 1236 <u>https://doi.org/10.1021/es300285d</u>
- Liu, D., Whitehead, J., Alfarra, M. R., Reyes-Villegas, E., Spracklen, D. V., Reddington, C. L., Kong, S.,
- 1238 Williams, P. I., Ting, Y.-C., Haslett, S., Taylor, J. W., Flynn, M. J., Morgan, W. T., McFiggans, G., Coe, H., &
- 1239 Allan, J. D. (2017). Black-carbon absorption enhancement in the atmosphere determined by particle
- mixing state. *Nature Geoscience*, 10(3), 184–188. https://doi.org/10.1038/ngeo2901
- 1241 Liu, J., Bergin, M., Guo, H., King, L., Kotra, N., Edgerton, E., & Weber, R. J. (2013). Size-resolved
- 1242 measurements of brown carbon in water and methanol extracts and estimates of their contribution to
- 1243 ambient fine-particle light absorption. Atmospheric Chemistry and Physics, 13(24), 12389–12404.
- 1244 <u>https://doi.org/10.5194/acp-13-12389-2013</u>
- Liu, S., Aiken, A. C., Gorkowski, K., Dubey, M. K., Cappa, C. D., Williams, L. R., Herndon, S. C., Massoli,
- 1246 P., Fortner, E. C., Chhabra, P. S., Brooks, W. A., Onasch, T. B., Jayne, J. T., Worsnop, D. R., China, S.,

- 1247 Sharma, N., Mazzoleni, C., Xu, L., Ng, N. L., ... Prévôt, A. S. H. (2015). Enhanced light absorption by
- mixed source black and brown carbon particles in UK winter. *Nature Communications*, 6.
- 1249 <u>https://doi.org/10.1038/ncomms9435</u>
- Lu, Z., Streets, D. G., Winijkul, E., Yan, F., Chen, Y., Bond, T. C., Feng, Y., Dubey, M. K., Liu, S., Pinto, J. P.,
- 4 Carmichael, G. R. (2015). Light absorption properties and radiative effects of primary organic aerosol
- emissions. Environmental Science and Technology, 49(8), 4868–4877.
- 1253 <u>https://doi.org/10.1021/acs.est.5b00211</u>
- Ma, J., Li, X., Gu, P., Dallmann, T. R., Presto, A. A., & Donahue, N. M. (2016). Estimating ambient
- 1255 particulate organic carbon concentrations and partitioning using thermal optical measurements and
- the volatility basis set. *Aerosol Science and Technology*, 50(6), 638–651.
- 1257 <u>https://doi.org/10.1080/02786826.2016.1158778</u>
- Martinsson, J., Eriksson, A. C., Nielsen, I. E., Malmborg, V. B., Ahlberg, E., Andersen, C., Lindgren, R.,
- 1259 Nyström, R., Nordin, E. Z., Brune, W. H., Svenningsson, B., Swietlicki, E., Boman, C., & Pagels, J. H.
- 1260 (2015). Impacts of Combustion Conditions and Photochemical Processing on the Light Absorption of
- 1261 Biomass Combustion Aerosol. *Environmental Science and Technology*, 49(24), 14663–14671.
- 1262 <u>https://doi.org/10.1021/acs.est.5b03205</u>
- 1263 McCarty, J. L., Aalto, J., Paunu, V.-V., Arnold, S. R., Eckhardt, S., Klimont, Z., Fain, J. J., Evangeliou, N.,
- 1264 Venäläinen, A., Tchebakova, N. M., Parfenova, E. I., Kupiainen, K., Soja, A. J., Huang, L., & Wilson, S.
- 1265 (2021). Reviews and syntheses: Arctic fire regimes and emissions in the 21st century. Biogeosciences,
- 1266 18(18), 5053–5083. https://doi.org/10.5194/bg-18-5053-2021
- 1267 McClure, C. D., Lim, C. Y., Hagan, D. H., Kroll, J. H., & Cappa, C. D. (2020). Biomass-burning-derived
- particles from a wide variety of fuels Part 1: Properties of primary particles. *Atmospheric Chemistry*
- 1269 and Physics, 20(3), 1531–1547. https://doi.org/10.5194/acp-20-1531-2020
- 1270 McIntyre, C., & McRae, C. (2005). Proposed guidelines for sample preparation and ESI-MS analysis of
- 1271 humic substances to avoid self-esterification. *Organic Geochemistry*, 36(4), 543–553.
- 1272 <u>https://doi.org/10.1016/j.orggeochem.2004.11.002</u>
- 1273 McMeeking, G. R., Fortner, E., Onasch, T. B., Taylor, J. W., Flynn, M., Coe, H., & Kreidenweis, S. M.
- 1274 (2014). Impacts of nonrefractory material on light absorption by aerosols emitted from biomass
- 1275 burning. Journal of Geophysical Research: Atmospheres, 119(21), 12,272-12,286.
- 1276 <u>https://doi.org/10.1002/2014JD021750</u>
- 1277 McRee, M. M., Moschos, V., Fiddler, M. N., Massabò, D., Surratt, J. D., & Bililign, S. (2025). Influence of
- relative humidity and aging on the optical properties of organic aerosols from burning African biomass
- 1279 fuels. Aerosol Science and Technology, 59(5), 544–566.
- 1280 https://doi.org/10.1080/02786826.2024.2412652
- 1281 Mo, Y., Li, J., Liu, J., Zhong, G., Cheng, Z., Tian, C., Chen, Y., & Zhang, G. (2017). The influence of solvent
- 1282 and pH on determination of the light absorption properties of water-soluble brown carbon.
- 1283 Atmospheric Environment, 161, 90–98. https://doi.org/10.1016/j.atmosenv.2017.04.037
- Moosmüller, H., Chakrabarty, R. K., & Arnott, W. P. (2009). Aerosol light absorption and its
- measurement: A review. Journal of Quantitative Spectroscopy and Radiative Transfer, 110(11), 844–
- 1286 878. https://doi.org/10.1016/j.jqsrt.2009.02.035

- Moosmüller, H., Chakrabarty, R. K., Ehlers, K. M., & Arnott, W. P. (2011). Absorption Ångström
- 1288 coefficient, brown carbon, and aerosols: Basic concepts, bulk matter, and spherical particles.
- 1289 Atmospheric Chemistry and Physics, 11(3), 1217–1225. https://doi.org/10.5194/acp-11-1217-2011
- Moschos, V., Christensen, C., Mouton, M., Fiddler, M. N., Isolabella, T., Mazzei, F., Massabò, D., Turpin,
- 1291 B. J., Bililign, S., & Surratt, J. D. (2024). Quantifying the Light-Absorption Properties and Molecular
- 1292 Composition of Brown Carbon Aerosol from Sub-Saharan African Biomass Combustion.
- 1293 Environmental Science and Technology, 58(9), 4268–4280. https://doi.org/10.1021/acs.est.3c09378
- Moschos, V., Kumar, N. K., Daellenbach, K. R., Baltensperger, U., Prévôt, A. S. H., & El Haddad, I.
- 1295 (2018). Source Apportionment of Brown Carbon Absorption by Coupling Ultraviolet-Visible
- 1296 Spectroscopy with Aerosol Mass Spectrometry. Environmental Science & Technology Letters, 5(6),
- 1297 302–308. https://doi.org/10.1021/acs.estlett.8b00118
- 1298 Mukherjee, A., Dey, S., Rana, A., Jia, S., Banerjee, S., & Sarkar, S. (2020). Sources and atmospheric
- 1299 processing of brown carbon and HULIS in the Indo-Gangetic Plain: Insights from compositional
- 1300 analysis. Environmental Pollution, 267. https://doi.org/10.1016/j.envpol.2020.115440
- 1301 Mukherjee, A., Hartikainen, A., Joutsensaari, J., Basnet, S., Mesceriakovas, A., Ihalainen, M., Yli-Pirilä,
- 1302 P., Leskinen, J., Somero, M., Louhisalmi, J., Fang, Z., Kalberer, M., Rudich, Y., Tissari, J., Czech, H.,
- 1303 Zimmermann, R., & Sippula, O. (2024). Black carbon and particle lung-deposited surface area in
- 1304 residential wood combustion emissions: Effects of an electrostatic precipitator and photochemical
- aging. Science of The Total Environment, 952, 175840.
- 1306 <u>https://doi.org/10.1016/j.scitotenv.2024.175840</u>
- 1307 Navinya, C., Kapoor, T. S., Anurag, G., Venkataraman, C., Phuleria, H. C., & Chakrabarty, R. K. (2024).
- 1308 Brownness of Organics in Anthropogenic Biomass Burning Aerosols over South Asia.
- 1309 <u>https://doi.org/10.5194/egusphere-2024-1313</u>
- 1310 Park, S. S., & Yu, J. (2016). Chemical and light absorption properties of humic-like substances from
- 1311 biomass burning emissions under controlled combustion experiments. Atmospheric Environment,
- 1312 136, 114–122. https://doi.org/10.1016/j.atmosenv.2016.04.022
- 1313 Phillips, C. A., Rogers, B. M., Elder, M., Cooperdock, S., Moubarak, M., Randerson, J. T., & Frumhoff, P.
- 1314 C. (2022). Escalating carbon emissions from North American boreal forest wildfires and the climate
- mitigation potential of fire management. *Science Advances*, 8(17).
- 1316 <u>https://doi.org/10.1126/sciadv.abl7161</u>
- 1317 Phillips, S. M., & Smith, G. D. (2017). Spectroscopic comparison of water- and methanol-soluble
- brown carbon particulate matter. *Aerosol Science and Technology*, 51(9), 1113–1121.
- 1319 https://doi.org/10.1080/02786826.2017.1334109
- 1320 Pokhrel, R. P., Wagner, N. L., Langridge, J. M., Lack, D. A., Jayarathne, T., Stone, E. A., Stockwell, C. E.,
- 1321 Yokelson, R. J., & Murphy, S. M. (2016). Parameterization of single-scattering albedo (SSA) and
- 1322 absorption Ångström exponent (AAE) with EC / OC for aerosol emissions from biomass burning.
- 1323 Atmospheric Chemistry and Physics, 16(15), 9549–9561. https://doi.org/10.5194/acp-16-9549-2016
- Pokhrel, R. P., Gordon, J., Fiddler, M. N., & Bililign, S. (2021). Impact of combustion conditions on
- 1325 physical and morphological properties of biomass burning aerosol. Aerosol Science and Technology,
- 1326 55(1), 80–91. https://doi.org/10.1080/02786826.2020.1822512
- Popovicheva, O. B., Engling, G., Ku, I.-T., Timofeev, M. A., & Shonija, N. K. (2019). Aerosol Emissions
- 1328 from Long-lasting Smoldering of Boreal Peatlands: Chemical Composition, Markers, and

- 1329 Microstructure. Aerosol and Air Quality Research, 19(3), 484–503.
- 1330 <u>https://doi.org/10.4209/aaqr.2018.08.0302</u>
- 1331 Rogers, B. M., Soja, A. J., Goulden, M. L., & Randerson, J. T. (2015). Influence of tree species on
- 1332 continental differences in boreal fires and climate feedbacks. *Nature Geoscience*, 8(3), 228–234.
- 1333 <u>https://doi.org/10.1038/ngeo2352</u>
- Rüger, C. P., Le Maître, J., Riches, E., Palmer, M., Orasche, J., Sippula, O., Jokiniemi, J., Afonso, C.,
- 1335 Giusti, P., & Zimmermann, R. (2021). Cyclic Ion Mobility Spectrometry Coupled to High-Resolution
- 1336 Time-of-Flight Mass Spectrometry Equipped with Atmospheric Solid Analysis Probe for the Molecular
- 1337 Characterization of Combustion Particulate Matter. Journal of the American Society for Mass
- 1338 Spectrometry, 32(1), 206–217. https://doi.org/10.1021/jasms.0c00274
- 1339 Saleh, R. (2020). From Measurements to Models: Toward Accurate Representation of Brown Carbon in
- 1340 Climate Calculations. In *Current Pollution Reports* (Vol. 6, Issue 2, pp. 90–104). Springer.
- 1341 <u>https://doi.org/10.1007/s40726-020-00139-3</u>
- 1342 Saleh, R., Cheng, Z., & Atwi, K. (2018). The Brown-Black Continuum of Light-Absorbing Combustion
- 1343 Aerosols. Environmental Science and Technology Letters, 5(8), 508–513.
- 1344 <u>https://doi.org/10.1021/acs.estlett.8b00305</u>
- 1345 Saleh, R., Robinson, E. S., Tkacik, D. S., Ahern, A. T., Liu, S., Aiken, A. C., Sullivan, R. C., Presto, A. A.,
- 1346 Dubey, M. K., Yokelson, R. J., Donahue, N. M., & Robinson, A. L. (2014). Brownness of organics in
- aerosols from biomass burning linked to their black carbon content. Nature Geoscience, 7(9), 647–
- 1348 650. https://doi.org/10.1038/ngeo2220
- 1349 Schneider, E., Rüger, C. P., Chacón-Patiño, M. L., Somero, M., Ruppel, M. M., Ihalainen, M., Köster, K.,
- 1350 Sippula, O., Czech, H., & Zimmermann, R. (2024a). The complex composition of organic aerosols
- 1351 emitted during burning varies between Arctic and boreal peat. Communications Earth and
- 1352 Environment, 5(1). https://doi.org/10.1038/s43247-024-01304-y
- 1353 Schneider, E., Czech, H., Hartikainen, A., Hansen, H. J., Gawlitta, N., Ihalainen, M., Yli-Pirilä, P.,
- 1354 Somero, M., Kortelainen, M., Louhisalmi, J., Orasche, J., Fang, Z., Rudich, Y., Sippula, O., Rüger, C. P., &
- 1355 Zimmermann, R. (2024b). Molecular composition of fresh and aged aerosols from residential wood
- 1356 combustion and gasoline car with modern emission mitigation technology. *Environmental Science*:
- 1357 Processes & Impacts, 26(8), 1295–1309. https://doi.org/10.1039/D4EM00106K
- 1358 Sedlacek, A. J., Buseck, P. R., Adachi, K., Onasch, T. B., Springston, S. R., & Kleinman, L. (2018).
- 1359 Formation and evolution of tar balls from northwestern US wildfires. Atmospheric Chemistry and
- 1360 Physics, 18(15), 11289–11301. https://doi.org/10.5194/acp-18-11289-2018
- 1361 Seinfeld, J.H. and Pandis, S.N. (2006) Atmospheric Chemistry and Physics: From Air Pollution to
- 1362 Climate Change. 2nd Edition, John Wiley & Sons, New York.
- 1363 Sengupta, D., Samburova, V., Bhattarai, C., Kirillova, E., Mazzoleni, L., Iaukea-Lum, M., Watts, A.,
- 1364 Moosmüller, H., & Khlystov, A. (2018). Light absorption by polar and non-polar aerosol compounds
- from laboratory biomass combustion. *Atmospheric Chemistry and Physics*, *18*(15), 10849–10867.
- 1366 <u>https://doi.org/10.5194/acp-18-10849-2018</u>
- 1367 Selimovic, V., Yokelson, R. J., Warneke, C., Roberts, J. M., de Gouw, J., Reardon, J., & Griffith, D. W. T.
- 1368 (2018). Aerosol optical properties and trace gas emissions by PAX and OP-FTIR for laboratory-
- 1369 simulated western US wildfires during FIREX. Atmospheric Chemistry and Physics, 18(4), 2929–2948.
- 1370 <u>https://doi.org/10.5194/acp-18-2929-2018</u>

- 1371 Shetty, N. J., Pandey, A., Baker, S., Hao, W. M., & Chakrabarty, R. K. (2019). Measuring light absorption
- by freshly emitted organic aerosols: Optical artifacts in traditional solvent-extraction-based methods.
- 1373 Atmospheric Chemistry and Physics, 19(13), 8817–8830. https://doi.org/10.5194/acp-19-8817-2019
- 1374 Smith, D. M., Fiddler, M. N., Pokhrel, R. P., & Bililign, S. (2020). Laboratory studies of fresh and aged
- 1375 biomass burning aerosol emitted from east African biomass fuels Part 1: Optical properties.
- 1376 Atmospheric Chemistry and Physics, 20(17), 10149–10168. https://doi.org/10.5194/acp-20-10149-
- 1377 2020
- 1378 Solum, M. S., Sarofim, A. F., Pugmire, R. J., Fletcher, T. H., & Zhang, H. (2001). 13 C NMR Analysis of
- 1379 Soot Produced from Model Compounds and a Coal. Energy & Fuels, 15(4), 961–971.
- 1380 <u>https://doi.org/10.1021/ef0100294</u>
- 1381 Stockwell, C. E., Jayarathne, T., Cochrane, M. A., Ryan, K. C., Putra, E. I., Saharjo, B. H., Nurhayati, A.
- D., Albar, I., Blake, D. R., Simpson, I. J., Stone, E. A., & Yokelson, R. J. (2016). Field measurements of
- 1383 trace gases and aerosols emitted by peat fires in Central Kalimantan, Indonesia, during the 2015 El
- 1384 Niño. Atmospheric Chemistry and Physics, 16(18), 11711–11732. https://doi.org/10.5194/acp-16-
- 1385 11711-2016
- 1386 Stockwell, C. E., Veres, P. R., Williams, J., & Yokelson, R. J. (2015). Characterization of biomass burning
- 1387 emissions from cooking fires, peat, crop residue, and other fuels with high-resolution proton-transfer-
- reaction time-of-flight mass spectrometry. *Atmospheric Chemistry and Physics*, 15(2), 845–865.
- 1389 <u>https://doi.org/10.5194/acp-15-845-2015</u>
- 1390 Stockwell, C. E., Yokelson, R. J., Kreidenweis, S. M., Robinson, A. L., DeMott, P. J., Sullivan, R. C.,
- 1391 Reardon, J., Ryan, K. C., Griffith, D. W. T., & Stevens, L. (2014). Trace gas emissions from combustion of
- peat, crop residue, domestic biofuels, grasses, and other fuels: configuration and Fourier transform
- 1393 infrared (FTIR) component of the fourth Fire Lab at Missoula Experiment (FLAME-4). Atmospheric
- 1394 Chemistry and Physics, 14(18), 9727–9754. https://doi.org/10.5194/acp-14-9727-2014
- 1395 Sumlin, B. J., Heinson, Y. W., Shetty, N., Pandey, A., Pattison, R. S., Baker, S., Hao, W. M., &
- 1396 Chakrabarty, R. K. (2018). UV–Vis–IR spectral complex refractive indices and optical properties of
- 1397 brown carbon aerosol from biomass burning. Journal of Quantitative Spectroscopy and Radiative
- 1398 *Transfer*, 206, 392–398. <u>https://doi.org/10.1016/j.jqsrt.2017.12.009</u>
- Sumlin, B. J., Pandey, A., Walker, M. J., Pattison, R. S., Williams, B. J., & Chakrabarty, R. K. (2017).
- 1400 Atmospheric Photooxidation Diminishes Light Absorption by Primary Brown Carbon Aerosol from
- 1401 Biomass Burning. Environmental Science & Technology Letters, 4(12), 540–545.
- 1402 <u>https://doi.org/10.1021/acs.estlett.7b00393</u>
- Taylor, N. F., Collins, D. R., Lowenthal, D. H., McCubbin, I. B., Hallar, A. G., Samburova, V., Zielinska, B.,
- 1404 Kumar, N., & Mazzoleni, L. R. (2017). Hygroscopic growth of water soluble organic carbon isolated
- 1405 from atmospheric aerosol collected at US national parks and Storm Peak Laboratory. Atmospheric
- 1406 Chemistry and Physics, 17(4), 2555–2571. https://doi.org/10.5194/acp-17-2555-2017
- 1407 Urbanski, S. P. (2013). Combustion efficiency and emission factors for wildfire-season fires in mixed
- 1408 conifer forests of the northern Rocky Mountains, US. Atmospheric Chemistry and Physics, 13(14),
- 1409 7241–7262. https://doi.org/10.5194/acp-13-7241-2013
- 1410 Vakkari, V., Kerminen, V., Beukes, J. P., Tiitta, P., Zyl, P. G., Josipovic, M., Venter, A. D., Jaars, K.,
- 1411 Worsnop, D. R., Kulmala, M., & Laakso, L. (2014). Rapid changes in biomass burning aerosols by

- 1412 atmospheric oxidation. Geophysical Research Letters, 41(7), 2644–2651.
- 1413 <u>https://doi.org/10.1002/2014GL059396</u>
- 1414 Vakkari, V., Beukes, J. P., Dal Maso, M., Aurela, M., Josipovic, M., & van Zyl, P. G. (2018). Major
- 1415 secondary aerosol formation in southern African open biomass burning plumes. Nature Geoscience,
- 1416 11(8), 580–583. https://doi.org/10.1038/s41561-018-0170-0
- 1417 Vakkari, V., Vettikkat, L., Kommula, S., Mukherjee, A., Hao, L., Backman, J., Buchholz, A., Gawlitta, N.,
- 1418 Ihalainen, M., Jaars, K., Köster, K., Le, V., Miettinen, P., Nissinen, A., Czech, H., Alton, M., Passig, J.,
- 1419 Peltokorpi, S., Piedehierro, A. A., Pullinen, I., Rosewig, E. I., Schobesberger, S., Shukla, D., Siebert, S.
- 1420 J., Somero, M., Virkkula, A., Welti, A., Yli-Pirilä, P., Ylisirniö, A., Zimmermann, R., van Zyl, P. G.,
- 1421 Virtanen, A., & Sippula, O. (2025). Laboratory experiments on savannah and European boreal forest
- 1422 fire emissions. Journal of Geophysical Research: Atmospheres, under revision
- van der Werf, G. R., Randerson, J. T., Giglio, L., van Leeuwen, T. T., Chen, Y., Rogers, B. M., Mu, M., van
- Marle, M. J. E., Morton, D. C., Collatz, G. J., Yokelson, R. J., & Kasibhatla, P. S. (2017). Global fire
- emissions estimates during 1997–2016. *Earth System Science Data*, 9(2), 697–720.
- 1426 <u>https://doi.org/10.5194/essd-9-697-2017</u>
- van Wees, D., van der Werf, G. R., Randerson, J. T., Rogers, B. M., Chen, Y., Veraverbeke, S., Giglio, L., &
- 1428 Morton, D. C. (2022). Global biomass burning fuel consumption and emissions at 500 m spatial
- resolution based on the Global Fire Emissions Database (GFED). Geoscientific Model Development,
- 1430 *15*(22), 8411–8437. <u>https://doi.org/10.5194/gmd-15-8411-2022</u>
- 1431 Walker, X. J., Rogers, B. M., Veraverbeke, S., Johnstone, J. F., Baltzer, J. L., Barrett, K., Bourgeau-Chavez,
- L., Day, N. J., de Groot, W. J., Dieleman, C. M., Goetz, S., Hoy, E., Jenkins, L. K., Kane, E. S., Parisien, M.-
- 1433 A., Potter, S., Schuur, E. A. G., Turetsky, M., Whitman, E., & Mack, M. C. (2020). Fuel availability not fire
- 1434 weather controls boreal wildfire severity and carbon emissions. Nature Climate Change, 10(12), 1130–
- 1435 1136. https://doi.org/10.1038/s41558-020-00920-8
- 1436 Wang, H. (2011). Formation of nascent soot and other condensed-phase materials in flames.
- 1437 Proceedings of the Combustion Institute, 33(1), 41–67. https://doi.org/10.1016/j.proci.2010.09.009
- 1438 Wang, Y., Hu, M., Xu, N., Qin, Y., Wu, Z., Zeng, L., Huang, X., & He, L. (2020). Chemical composition
- 1439 and light absorption of carbonaceous aerosols emitted from crop residue burning: Influence of
- 1440 combustion efficiency. *Atmospheric Chemistry and Physics*, 20(22), 13721–13734.
- 1441 https://doi.org/10.5194/acp-20-13721-2020
- 1442 Washenfelder, R. A., Attwood, A. R., Brock, C. A., Guo, H., Xu, L., Weber, R. J., Ng, N. L., Allen, H. M.,
- Ayres, B. R., Baumann, K., Cohen, R. C., Draper, D. C., Duffey, K. C., Edgerton, E., Fry, J. L., Hu, W. W.,
- 1444 Jimenez, J. L., Palm, B. B., Romer, P., ... Brown, S. S. (2015). Biomass burning dominates brown carbon
- absorption in the rural southeastern United States. Geophysical Research Letters, 42(2), 653–664.
- 1446 https://doi.org/10.1002/2014GL062444
- 1447 Wilson, D., Dixon, S. D., Artz, R. R. E., Smith, T. E. L., Evans, C. D., Owen, H. J. F., Archer, E., & Renou-
- 1448 Wilson, F. (2015). Derivation of greenhouse gas emission factors for peatlands managed for extraction
- in the Republic of Ireland and the United Kingdom. *Biogeosciences*, 12(18), 5291–5308.
- 1450 <u>https://doi.org/10.5194/bg-12-5291-2015</u>
- 1451 Wu, H., Taylor, J. W., Langridge, J. M., Yu, C., Allan, J. D., Szpek, K., Cotterell, M. I., Williams, P. I., Flynn,
- 1452 M., Barker, P., Fox, C., Allen, G., Lee, J., & Coe, H. (2021). Rapid transformation of ambient absorbing

- aerosols from West African biomass burning. *Atmospheric Chemistry and Physics*, 21(12), 9417–9440.
- 1454 <u>https://doi.org/10.5194/acp-21-9417-2021</u>
- 1455 Xie, M., Hays, M. D., & Holder, A. L. (2017). Light-absorbing organic carbon from prescribed and
- laboratory biomass burning and gasoline vehicle emissions. *Scientific Reports*, 7(1), 7318.
- 1457 https://doi.org/10.1038/s41598-017-06981-8
- 1458 Xie, M., Shen, G., Holder, A. L., Hays, M. D., & Jetter, J. J. (2018). Light absorption of organic carbon
- 1459 emitted from burning wood, charcoal, and kerosene in household cookstoves. Environmental
- 1460 *Pollution*, 240, 60–67. https://doi.org/10.1016/j.envpol.2018.04.085
- 1461 Xu, Z., Feng, W., Wang, Y., Ye, H., Wang, Y., Liao, H., & Xie, M. (2022). Potential underestimation of
- ambient brown carbon absorption based on the methanol extraction method and its impacts on
- 1463 source analysis. Atmospheric Chemistry and Physics, 22(20), 13739–13752.
- 1464 https://doi.org/10.5194/acp-22-13739-2022
- 1465 Yan, C., Zheng, M., Sullivan, A. P., Bosch, C., Desyaterik, Y., Andersson, A., Li, X., Guo, X., Zhou, T.,
- 1466 Gustafsson, Ö., & Collett, J. L. (2015). Chemical characteristics and light-absorbing property of water-
- 1467 soluble organic carbon in Beijing: Biomass burning contributions. Atmospheric Environment, 121, 4–
- 1468 12. https://doi.org/10.1016/j.atmosenv.2015.05.005
- 1469 Yan, F., Kang, S., Sillanpää, M., Hu, Z., Gao, S., Chen, P., Gautam, S., Reinikainen, S. P., & Li, C. (2020).
- 1470 A new method for extraction of methanol-soluble brown carbon: Implications for investigation of its
- light absorption ability. Environmental Pollution, 262. https://doi.org/10.1016/j.envpol.2020.114300
- 1472 Yokelson, R. J., Goode, J. G., Ward, D. E., Susott, R. A., Babbitt, R. E., Wade, D. D., Bertschi, I., Griffith,
- D. W. T., & Hao, W. M. (1999). Emissions of formaldehyde, acetic acid, methanol, and other trace gases
- 1474 from biomass fires in North Carolina measured by airborne Fourier transform infrared spectroscopy.
- 1475 Journal of Geophysical Research: Atmospheres, 104(D23), 30109–30125.
- 1476 <u>https://doi.org/10.1029/1999JD900817</u>
- 1477 Yokelson, R. J., Griffith, D. W. T., & Ward, D. E. (1996). Open-path Fourier transform infrared studies of
- 1478 large-scale laboratory biomass fires. Journal of Geophysical Research: Atmospheres, 101(D15),
- 1479 21067–21080. https://doi.org/10.1029/96JD01800
- 1480 Zeng, L., Dibb, J., Scheuer, E., Katich, J. M., Schwarz, J. P., Bourgeois, I., Peischl, J., Ryerson, T.,
- Warneke, C., Perring, A. E., Diskin, G. S., Digangi, J. P., Nowak, J. B., Moore, R. H., Wiggins, E. B.,
- 1482 Pagonis, D., Guo, H., Campuzano-Jost, P., Jimenez, J. L., ... Weber, R. J. (2022). Characteristics and
- evolution of brown carbon in western United States wildfires. Atmospheric Chemistry and Physics,
- 1484 *22*(12), 8009–8036. <u>https://doi.org/10.5194/acp-22-8009-2022</u>
- 1485 Zhang, Z., Wang, Y., Chen, X., Xu, L., Zheng, Z., Ching, J., Zhu, S., Liu, D., & Li, W. (2025). Absorption
- enhancement and shielding effect of brown organic coating on black carbon aerosols. *Npj Climate*
- 1487 and Atmospheric Science, 8(1). https://doi.org/10.1038/s41612-025-00989-y
- 1488 Zhao, B., Zhuang, Q., Shurpali, N., Köster, K., Berninger, F., & Pumpanen, J. (2021). North American
- boreal forests are a large carbon source due to wildfires from 1986 to 2016. Scientific Reports, 11(1),
- 1490 7723. https://doi.org/10.1038/s41598-021-87343-3
- 1491 Zhong, Q., Schutgens, N., Veraverbeke, S., & van der Werf, G. R. (2024). Increasing aerosol emissions
- 1492 from boreal biomass burning exacerbate Arctic warming. *Nature Climate Change*, 14(12), 1275–1281.
- 1493 <u>https://doi.org/10.1038/s41558-024-02176-y</u>

1494 1495	Appendix:	
1496	APM	Aerosol Particle Mass Analyzer
1497	ВВ	Biomass Burning
1498	ВС	Black Carbon
1499	BFS	Boreal forest Surface samples (from Finland)
1500	BrC	Brown Carbon
1501	СР	Commercial Peat samples (from Finland)
1502	DMF	Dimethylformamide
1503	DR	Dilution Ratio
1504	eBC	equivalent Black Carbon, approximated black carbon concentration by Aethalometer
1505	EC	Elemental Carbon
1506	EF	Emission Factor
1507	ELVOC	Extremely Low Volatility Organic Carbon
1508	FIA	Finnish boreal peatland (from Lakkasuo)
1509	FIB	Finnish boreal peatland (from Siikaneva)
1510	FTIR	Fourier-Transform InfraRed Spectrophotometer
1511	K	imaginary part of refractive inde
1512	MAE	Mass Absorption Efficiency
1513	MCE	Modified Combustion Efficiency
1514	MeOH	Methanol, an organic solvent
1515	MSOC	Methanol Soluble Organic Carbon
1516	NMVOC	Non-Methane Volatile Organic Carbon
1517	NOR	Arctic peatland samples (from Svalbard, Norway)
1518	OA	Organic aerosol
1519	OC	Organic Carbon, refers to only the carbon mass of OA
1520	PEAR	Photochemical Emission Aging flow-tube Reactor
1521	PM_1	Particulate matter with aerodynamic diameter of 1 µm or less
1522	PM ₁₀	Particulate matter with aerodynamic diameter of 1 µm or less
1523	POA	Primary Organic Aerosol
1524	POC	Primary Organic Carbon

1525	PRD	Porous Tube Dilutor
1526	UV	Ultra-violet, spectral region consisting light radiation wavelength of 100-400 nm
1527	OHR_{ext}	external reactivity of hydroxyl radicals
1528	RUS	peatland samples (from Rogovaya, Russia)
1529	RWC	Residential Wood Combustion
1530	SG	Savanna Grass (grassy savnna samples from South Africa)
1531	SMPS	Scanning Mobility Particle Sizer
1532	SOA	Secondary Organic Aerosol
1533	SOC	Secondary Organic Carbon
1534	SW	Savanna Wood (woody savanna biomass from South Africa)
1535	TOC	Total Organic Carbon
1536	CPC	Condensation Particle Counter
1537	DMA	Differential Mobility Analyzer
1538	SEM	Scanning Electron Microscopy
1539	WSOC	Water Soluble Organic Carbon